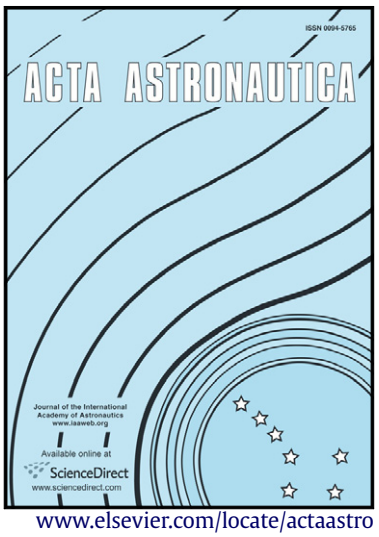

www.elsevier.com/locate/actaastro

Eddy Currents applied to De-tumbling of Space Debris: Analysis and Validation of Approximate Proposed Methods

Natalia Ortiz Gómez, Scott J.I. Walker

PII: S0094-5765(15)00168-X
DOI: http://dx.doi.org/10.1016/j.actaastro.2015.04.012
Reference: AA5414

To appear in: *Acta Astronautica*

Received date: 19 October 2014
Revised date: 23 March 2015
Accepted date: 16 April 2015

Cite this article as: Natalia Ortiz Gómez, Scott J.I. Walker, Eddy Currents applied to De-tumbling of Space Debris: Analysis and Validation of Approximate Proposed Methods, *Acta Astronautica,* http://dx.doi.org/10.1016/j.actaastro.2015.04.012

Eddy Currents applied to De-tumbling of Space Debris: Analysis and Validation of Approximate Proposed Methods

Natalia Ortiz Gómez

Southampton University, Highfield SO17 1BJ United Kingdom

Dr. Scott J.I. Walker

Southampton University, Highfield SO17 1BJ United Kingdom

Abstract

The space debris population has greatly increased over the last few decades. Active debris removal (ADR) methods may become necessary to remove those objects in orbit that pose the biggest collision risk. Those ADR methods that require contact with the target, show complications if the target is rotating at high speeds. Observed rotations can be higher than 60 deg/s combined with precession and nutation motions. "Natural" rotational damping in upper stages has been observed for some space debris objects. This phenomenon occurs due to the eddy currents induced by the Earth's magnetic field in the predominantly conductive materials of these man made rotating objects. Existing solutions for the analysis of eddy currents require time-consuming finite element models to solve a Poisson equation throughout the volume. The first part of this paper presents a new method to compute the eddy current torque based on the computation of a new tensor called the 'Magnetic Tensor'. The general theory to compute this tensor by Finite Element Method is given as well as a particular Frame Model. This last model enables an explicit formula to be determined to evaluate the magnetic tensor. Analytical solutions for the spherical shell, the open cylinder and flat plates are given for the magnetic tensor and the eddy current torque model is validated with existing published work. The second part of the paper presents an active de-tumbling method for space debris objects based on eddy currents. The braking method that is proposed has the advantage of avoiding any kind of mechanical contact with the target. The space debris object is subjected to an enhanced magnetic field created from a chaser spacecraft which has one or more deployable structures with an electromagnetic coil at its end. The braking time and the possible induced precession is analysed for a metallic spherical shell considering different ratios of conductive vs. non-conductive material. The paper finalises with a case study based on the de-tumbling of an Ariane-4 Upper Stage H10 under the effect of the gravity gradient and a preliminary analysis of the non-uniformity of the magnetic field is presented.

Keywords: Active debris removal; Earth's magnetic field; Eddy currents; Tumbling

1. Introduction

The total number of tracked objects in Earth orbit above 10 cm in size exceeds 21000 (NASA Orbital Debris Program Office, 2014). Particles between 1 and 10 cm in size are estimated to be 500,000 and particles smaller than 1 cm are estimated to be above 100 million (NASA Orbital Debris Program Office, 2014). At present, every new Earth mission needs to allocate a certain amount of propellant for collision avoidance manoeuvres and these manoeuvres have become more frequent over the years (La Porte & Sasot, 2008). In addition, the average estimated collision rate per year in mid-2013 was 0.24 (i.e. 1 collision every 5 years) (Pardini & Anselmo, 2014) . In the coming years, Active Debris Removal (ADR) methods may become necessary to remove those objects in orbit that pose the biggest risk.

Current active debris removal methods can be divided into contact and contactless methods for complete removal (Bonnal et al., 2013; Innocenti et al., 2013). Non-contact methods have some advantages with respect to contact methods because all problems related to the grabbing of a non-cooperative target are avoided. However, contactless methods lead to an uncontrolled re-entry which is only adequate for de-orbiting small targets which will disintegrate in the atmosphere or for re-orbiting them to a graveyard orbit.

The controlled re-entry of large objects requires the use of chemical propulsion for the de-orbiting phase. This can be achieved with contact ADR methods which grab the space debris object by means of a rigid or flexible capture system and de-orbit the combined system in a con-

Email addresses: N.Ortiz-Gomez@soton.ac.uk (Natalia Ortiz Gómez), sjiw@soton.ac.uk (Dr. Scott J.I. Walker)

trolled way. Examples of proposed rigid capture systems are tentacles or a robotic arm. Examples of flexible capture systems are a net, harpoon or clamp. All these methods have applicability limitations depending on the rotational motion of the target. For instance, the maximum rotational speed that can be stopped by current robotic arms is around 4-5 degrees/sec (Castronuovo, 2011).

However, even if the target is rotating at a lower speed, it may be difficult to achieve zero relative angular velocity between the chaser and the target if the non-cooperative object has a complex motion, such as a rotation about all three axes. This aspect is not well tackled in the literature as the capture process is usually analysed for targets that are rotating about 1 axis.

Dealing with tumbling objects using flexible capture systems is still an open point. In the case of a harpoon or a net, there exists the risk of an entanglement between the tether and the target if the rotational motion of the target is not stabilized. Some papers claim that once the target is captured, the tension achieved on the tether with impulsive thrusts during the de-orbiting phase will help to control the rotational motion of the target (Jaspera & Schaubb, 2014; Wormnes et al., 2013).

Due to the limitations of the proposed contact ADR methods, a de-tumbling phase prior to the grabbing phase may be needed.

The present article focuses on the analysis of a contactless de-tumbling method based on eddy currents which was first proposed by Kadaba (Kadaba, 1995). Little work has been carried out afterwards on this idea (Fuhimito, 2012) and this article deepens on the mathematical models that drive this phenomenon as well as some aspects of the mission design. The main objective of the present work is to provide with the necessary mathematical expressions to analyse the orbital and rotational dynamics of the chaser-target system (forces and torques) due to the eddy current phenomenon, in an approximate but direct way. The article is organised as follows. Section 3 presents a deep analysis on the mathematical models of the eddy currents phenomenon. The major contribution of this paper is the introduction of a new tensor called the 'Magnetic Tensor' which provides us with a direct formula to evaluate the torque induced by the eddy currents when the magnetic field is homogeneous and constant. This way, it is possible to avoid solving the Poisson equation with Neumann conditions, for any type of conductive solid, in each time step of the integration of Euler equations. Section 3.3 includes a method to evaluate this tensor based on a generic Finite Element Method and Section 3.3.1 is particularised for a specific F.E.M. (Frame Model) which leads to a direct formula to evaluate this tensor. In addition, analytical solutions of this tensor are presented and compared with existing solutions for the eddy current torque (Smith, 1962; Ormsby, 1967) (Section 3.4).

Symbol	Quantity	Unit
A	Area	m^2
$\vec{B}$	Magnetic Field vector	T
E	Energy	J
$\vec{E}$	Electric Field vector	V m^{-1}
e	Thickness	m
f	Force	N
I	Inertia Tensor	kg m^2
J	Electric Intensity	A
$\vec{j}$	Electric Current Density vector	A m^{-2}
K	Stiffness matrix	N V^{-1}
L	Length	m
M	Magnetic Tensor	S m^4
$\vec{m}$	Magnetic Moment	A m^2
R	Radius	m
$\vec{T}$	Torque	N m
ϵ	Electric Permittivity	F m^{-1}
ε	Electromotive Force	V
Λ	Jacobian matrix	T m^{-1}
μ	Magnetic Permeability	H m^{-1}
$\vec{\omega}$	Angular Velocity vector	rad s^{-1}
ϕ	Electric potential	V
ψ	Potential	V
φ	Magnetic flux	V s
σ	Conductivity	S m^{-1}
τ	Characteristic Time	s

Table 1: Nomenclature.

The second part of the paper presents a preliminary analysis of an active contactless de-tumbling method based on eddy currents (Section 4). The process will be done actively with a chaser spacecraft which has one or more magnetic coils. Sections (Sections 4.3, 4.4) analyse the characteristic time of decay of the process for different percentages of conductive material and the precession induced under the assumption of a constant (no time variation) and homogeneous magnetic field. Section 4.5 presents a case study based on the Ariane 4 upper stage under the same assumption. Finally, Section 4.6 explains the main consequences of having a spatial gradient on the magnetic field which result in an efficiency penalty in the method and the appearance of net forces between the chaser and the target object.

2. Nomenclature

The nomenclature used in this paper can be found in Table 2.

3. Eddy Currents Analysis

The rotational dynamics of a rigid body can be studied using Euler equations (Hughes, 2004). The advantage of these equations is that they are expressed in a fixed frame to the rigid body (body reference frame) and therefore,

the inertia tensor is constant in this reference frame. The body reference frame used in this paper, has its origin at the center of gravity (COG) of the target and its axes go along the principal inertia axes of the body. Equation (1) shows Euler equations where $\vec{\omega}$ is the angular velocity vector between an inertial reference frame and the body frame, I is the inertia tensor and $\sum \vec{T}$ are all the applied torques.

$$I\dot{\vec{\omega}} + (\vec{\omega} \times I\vec{\omega}) = \sum \vec{T}. \tag{1}$$

When there is a rotating conductive body in the presence of a magnetic field, loop electric currents are induced due to Lenz's Law and they are called Eddy currents (Landau & Lifshitz, 1984). These currents induce torques on the rotating body which decrease its rotational speed and they may also cause a precession of the axis of rotation. Most spacecraft contain metallic structures and this phenomenon takes place at Low Earth Orbits (LEO) due to the Earth's magnetic field (Williams & Meadows, 1978; Yu, 1963; Boehnhardt et al., 1989).

From now on, it will be assumed that the rotating body is a rigid body and the magnetic field is constant and uniform $\vec{B}(\vec{r}, t) = constant$. In addition, the conductive materials considered have a relative permeability close to 1. This is the case of typical metallic materials used on spacecraft such as aluminum or titanium. The equations that describe this phenomenon are (Landau & Lifshitz, 1984; Praly et al., 2012):

$$\nabla \cdot \vec{j} = 0 \ \ \forall P \in V, \tag{2}$$

$$\nabla \times \vec{j} = \sigma(\vec{\omega} \times \vec{B}) = \sigma\vec{\Omega} \ \ \forall P \in V, \tag{3}$$

$$\vec{j} \cdot \vec{n}_v = 0 \ \ \forall P \in \partial V, \tag{4}$$

$\vec{j}$ is the electric current density vector that appears in the volume V, $\vec{\omega}$ is the angular velocity vector of the rigid body, $\vec{B}$ is the magnetic field, σ is the electrical conductivity of the body and $\vec{n}_v$ is the vector normal to the contour surface ∂V. In addition, the magnitude $\vec{\Omega} = \vec{\omega} \times \vec{B}$ is introduced in the equations.

Equation (2) is the continuity equation (Landau & Lifshitz, 1984; Vanderlinde, 2004) which describes the electric charge conservation inside the volume V. Here it was assumed that there is no accumulation of charge (Ormsby, 1967). In addition, Equation (3) is obtained by combining Maxwell's equation $\nabla \times \vec{E} = \vec{0}$ (for $\frac{\partial \vec{B}}{\partial t} = \vec{0}$) with Ohm's Law $\vec{j} = \sigma(\vec{E} + \vec{v} \times \vec{B})$, assuming that $\vec{B}(\vec{r}, t) = constant$. $\vec{E}$ is the electric field and $\vec{v} = \vec{\omega} \times \vec{r}$ is the velocity of each differential mass in the rigid body. Finally, Equation (4) describes the boundary conditions for $\vec{j}$ which must stay inside the volume.

The solution to this system of linear differential Equations (2,3,4) can be expressed as the sum of a particular solution and a homogeneous solution as shown in (5), where ψ is an unknown scalar function (Weinberger, 1995).

$$\vec{j} = \vec{j}_{part} - \sigma \cdot \nabla\psi. \tag{5}$$

Introducing (5) into Equation (3), it is found that the particular solution $\vec{j}_{part}$ must comply with Equation (6). Then, Equation (3) is immediately satisfied.

$$\nabla \times \vec{j}_{part} = \sigma(\vec{\omega} \times \vec{B}) = \sigma\vec{\Omega}. \tag{6}$$

3.1. Particular solutions for the current density vector

3.1.1. First particular solution. Classical formulation.

The classical way to express the current density vector is by choosing the particular solution $\vec{j}^{(1)}_{part} = \sigma(\vec{\omega} \times \vec{r}) \times \vec{B}$ (Landau & Lifshitz, 1984; Ormsby, 1967).

$$\vec{j} = \sigma(\vec{\omega} \times \vec{r}) \times \vec{B} - \sigma\nabla\phi. \tag{7}$$

Looking closer at Equation (7), it is deduced that it coincides with Ohm's Law and the scalar function ϕ corresponds to the electric potential $\vec{E} = -\nabla\phi$. Introducing solution (7) in the continuity Equation (2) and the boundary conditions (4), the following Poisson equation with Neumann conditions is obtained for ϕ (Praly et al., 2012):

$$\nabla^2\phi = \frac{2}{\sigma}\vec{\omega} \cdot \vec{B} \ \ \forall P \in V, \tag{8}$$

$$\frac{\partial\phi}{\partial n_v} = ((\vec{\omega} \times \vec{r}) \times \vec{B}) \cdot \vec{n}_v \ \ \forall P \in \partial V, \tag{9}$$

3.1.2. Second particular solution.

In some cases, it may be more convenient to choose a different particular solution. The proposed particular solution (10) leads to a Laplace Equation (12) instead of the non-homogeneous equation in partial derivatives (8). Consequently, this solution may approximate better to the real distribution of electric currents and it corresponds to the exact solution when the Neumann boundary conditions are null (e.g. spherical shell $\forall\vec{\Omega}$; cylindrical shell with $\vec{\Omega}$ along its axis; flat circular plate with $\vec{\Omega}$ perpendicular to its plane). In addition, this solution will be the key to obtain a direct formula for the Magnetic Tensor in Section 3.3.1.

$$\vec{j}^{(2)}_{part} = \frac{\sigma}{2}\vec{\Omega} \times \vec{r}. \tag{10}$$

In this case, the general solution for $\vec{j}$ is

$$\vec{j} = \frac{\sigma}{2}\vec{\Omega} \times \vec{r} - \sigma \cdot \nabla\psi. \tag{11}$$

This solution complies directly with Equation (3). Introducing (11) in the continuity Equation (2) and the boundary conditions (4), the following Laplace equation with Neumann boundary conditions is obtained for ψ:

$$\nabla^2\psi = 0 \ \ \forall P \in V, \tag{12}$$

$$\frac{\partial\psi}{\partial n_v} = -\frac{1}{2}(\vec{r} \times \vec{\Omega}) \cdot \vec{n}_v \ \ \forall P \in \partial V, \tag{13}$$

It must be highlighted that the scalar function ψ of the second particular solution does not correspond anymore to the conventional electric potential ϕ. Therefore, it will be called "effective potential".

This formulation introduces naturally the new parameter $\vec{\Omega} = \vec{\omega} \times \vec{B}$. Equations (2, 3, 4) and (12, 13) show the linearity of the solution of ψ and $\vec{j}$ with respect to this parameter $\vec{\Omega}$. This property will help to prove the existence of the Magnetic Tensor in Section (3.2).

3.2. The Magnetic Tensor

The general formula of the eddy current torque can be expressed as the cross product of the magnetic moment $\vec{m}$ and the magnetic field $\vec{B}$ (Landau & Lifshitz, 1984; Hughes, 2004; Vanderlinde, 2004),

$$\vec{T} = \vec{m} \times \vec{B}, \tag{14}$$

and the magnetic moment of the body is defined as (Landau & Lifshitz, 1984; Vanderlinde, 2004):

$$\vec{m} = \frac{1}{2} \int \vec{r} \times \vec{j} dV. \tag{15}$$

One general way to evaluate this torque would be to use a finite element method in order to divide the volume into a grid and solve the Laplace equation with Neumann boundary conditions (12, 13). Once the scalar function ψ is known, the current density vector $\vec{j}$ and therefore, the magnetic moment (15) and the torque (14) can be evaluated. The next step would be to integrate Euler Equations (1) in order to obtain the evolution of the angular velocity vector $\vec{\omega}$. It must be highlighted that the whole process would have to be repeated in each time step during the integration process of Euler equations, unless explicit direct formulae for the eddy current torque were obtained.

The fact that it is unpractical to solve the Neumann problem at each time step is already shown in previous articles (Smith, 1962; Ormsby, 1967; Praly et al., 2012), where specific formulae were obtained for the eddy current torque in some particular cases. As it will be proved in this section, the torque can be expressed in a general way by means of a tensor which will be called the *'Magnetic Tensor'* M. The concept of the Magnetic Tensor provides us with a general strategy to solve the problem for any type body. As it will be explained below, this tensor only depends on the physical properties (geometry and conductivity) of the body and it only needs to be computed once. When the magnetic tensor is known, the evaluation of the torque due to the eddy currents consists of a direct formula given by (18).

As it was explained in the previous section, the general solution for $\vec{j}$ is linear in $\vec{\Omega}$. If Equations (2, 3, 4) are solved for the three different cases, $\vec{\Omega}^{(1)} = \begin{bmatrix} 1 \\ 0 \\ 0 \end{bmatrix}$, $\vec{\Omega}^{(2)} = \begin{bmatrix} 0 \\ 1 \\ 0 \end{bmatrix}$, $\vec{\Omega}^{(3)} = \begin{bmatrix} 0 \\ 0 \\ 1 \end{bmatrix}$, a set of solutions for $\vec{j}^{(k)}(\vec{r})$ $(1 \leq k \leq 3)$ is obtained.

Taking into account the linearity with respect to $\vec{\Omega}$, the solution for $\vec{j}$ can be expressed for a given $\vec{\Omega} = \begin{bmatrix} \Omega_1 \\ \Omega_2 \\ \Omega_3 \end{bmatrix} = \sum_{i=1}^{n} \Omega_i \vec{\Omega}^{(i)}$ as:

$$\vec{j}(\vec{r}) = \sum_{k=1}^{3} \Omega_k \cdot \vec{j}^{(k)}(\vec{r}). \tag{16}$$

In addition, introducing (16) in (15), it is derived that the magnetic moment $\vec{m}$ is also linear in $\vec{\Omega}$ and it acquires the general form:

$$m_i = \sum_{j=1}^{3} M_{ij} \Omega_j, \quad 1 \leq j \leq 3. \tag{17}$$

Note that $\vec{j}(\vec{r})$ depends on $\vec{B}$ and $\vec{\omega}$ only through $\vec{\Omega} = \vec{\omega} \times \vec{B}$. Therefore, the components M_{ij} should be considered as proportionality 'constants' of the i-component of $\vec{m}$ with respect to the three components of $\vec{\Omega}$ and these components M_{ij} only depend on the geometry and conductivity of the body. The parameter M will be called 'Magnetic Tensor'.

Combining Equations (14) and (17), the torque induced by the eddy currents is:

$$\vec{T} = (M\vec{\Omega}) \times \vec{B}. \tag{18}$$

Next, the following properties of the Magnetic Tensor are proved:

1. *M is a cartesian tensor of second order*:

   $\vec{m}$ and $\vec{\Omega}$ are two vectors which can be transformed from an arbitrary cartesian reference to another using the corresponding rotation matrix R. These transformations can be expressed as:

   $$\begin{cases} \vec{m}' = R\vec{m} & \forall \vec{m} \\ \vec{\Omega}' = R\vec{\Omega} & \forall \vec{\Omega} \end{cases}. \tag{19}$$

   Entering into (17) $\vec{m}' = M'\vec{\Omega}' \Rightarrow R\vec{m} = M'R\vec{\Omega} \Rightarrow \vec{m}' = R^T M' R\vec{\Omega}' = M\vec{\Omega}'$. As the previous relationship holds $\forall \vec{\Omega}$ and its corresponding variable $\vec{m}$, it can be inferred that $M = R^T M' R$ or $M' = RMR^T$. Therefore, it can be concluded that M transforms as a cartesian tensor of second order.
2. *M has dimensions of* $[\mathrm{S{\cdot}m^4}]$ *being S the Siemens unit*:

   The units of the Magnetic Tensor can be derived from Equation (17) as the units of the magnetic moment $\vec{m}$ are $[\mathrm{A{\cdot}m^2}]$ and the units of $\vec{\Omega}$ are $[\mathrm{rad{\cdot}T/s}]$. Therefore the units of the Magnetic Tensor are:

   $$[\mathrm{s^3{\cdot}A^2m^2kg^{-1}{=}S{\cdot}m^4}].$$

3. *The dissipative energy per unit time due to the eddy currents has the form* $\dot{E} = -\vec{\Omega}^T M \vec{\Omega}$:

   The dissipated energy per unit time due to the eddy currents phenomenon is $\dot{E} = \vec{T} \cdot \vec{\omega}$. Using Equation (18), it can be found that:

$$\dot{E} = ((M\vec{\Omega}) \times \vec{B}) \cdot \vec{\omega} = (M\vec{\Omega}) \cdot (\vec{B} \times \vec{\omega}) = -\vec{\Omega}^T M \vec{\Omega}. \tag{20}$$

4. *The Magnetic Tensor is symmetric*:

   The symmetry of M is an important property because it will allow for its subsequent derivation from the energy dissipation balance. This symmetry can be deduced from Onsager's laws for irreversible processes (Reif, 1965).

   The currents $\vec{j}$ are responsible for the energy dissipation that will be later calculated applying Ohm's and Joule's laws, i.e., as a linearized irreversible process. Hence, Onsager's Reciprocal Relations apply and the symmetry of M is derived in a very straightforward way, as it is shown below.

   In the presence of an external magnetic field, Onsager's Law foresees two possible relations for M which are mutually exclusive:

$$\begin{cases} M_{ik}(\vec{H}) = M_{ki}(-\vec{H}) \text{ if both (or none) } \vec{m} \text{ and } \vec{\Omega} \\ \qquad\qquad \text{are proportional to velocities,} \\ M_{ik}(\vec{H}) = -M_{ki}(-\vec{H}) \text{ if velocities are only included} \\ \qquad\qquad \text{either in } \vec{m} \text{ or } \vec{\Omega}. \end{cases} \tag{21}$$

   Assuming that the relationship between the magnetic induction $\vec{B}$ and the magnetic field $\vec{H}$ is linear in μ (magnetic permeability), the previous relationships can be written as $M(\vec{B}) = \pm M^T(-\vec{B})$.

   As 'constants', the M_{ik} only depend on the geometry of the body; so they are not dependent on $\vec{B}$. For $M(\vec{B}) =$ constant, the above relation reduces to two possibilities:

$$\begin{cases} \text{A symmetric constant matrix } M = M^T \\ \text{Or an antisymmetric constant matrix } M = -M^T \end{cases} \tag{22}$$

   If M were antisymmetric, the dissipated energy per unit time would be zero $\dot{E} = 0$, $\forall\vec{\omega}$ and $\forall\vec{B}$, that is, the torque given by (18) would always be perpendicular to $\vec{\omega}$. This hypothesis contradicts the observed dissipative nature of the eddy currents phenomenon and therefore, it must be rejected. Instead, the other possibility quoted in (22) (M symmetric) allows for non-zero values of the quadratic form given by (20). This matches with the observed dissipative nature of the phenomenon if M has no negative eigenvalues (see next paragraph). Therefore, it can be concluded that M should be a symmetric tensor. Section (A) contains an additional self-contained mathematical proof of the symmetrical character of M.

5. *The Magnetic Tensor has no negative eigenvalues*:

   The eddy currents phenomenon is a dissipative effect which generates heat due to Joule's Law (Landau & Lifshitz, 1984). Hence, the derivative of the energy (in our case kinetic energy) must be $\dot{E} \leq 0$. From Equation (20), the previous condition leads to the quadratic form $\vec{\Omega}^T M \vec{\Omega} \geq 0$. This implies that the Magnetic Tensor has no negative eigenvalues. If none of the eigenvalues are zero, then the components of M form a symmetric definite positive 3×3 matrix.

Additional characteristics of the eddy currents phenomenon can be inferred from the torque formula given by (18).

1. The eddy current torque (18) is invariant under the change $\vec{B} \to -\vec{B}$ for a given $\vec{\omega}$. Therefore, when $\dot{E} < 0$, the component of $\vec{T}$ parallel to $\vec{\omega}$ will always oppose the velocity vector, no matter which sign of $\vec{B}$ is chosen.
2. For a given value of $\vec{\Omega}$, the maximum dissipation occurs when the orientation of $\vec{\Omega}$ coincides with the eigenvector that corresponds to the maximum eigenvalue of M.
3. If $\vec{\omega}$ is parallel to the magnetic field $\vec{B}$, then $\vec{\Omega} = \vec{0}$ and the torque is zero (18). Therefore, there is no dissipation of energy (20).
4. If $\vec{\omega} = \vec{\omega}_{||} + \vec{\omega}_{\perp}$ is composed of a parallel component to the magnetic field $\vec{\omega}_{||}$ and a perpendicular component to the magnetic field $\vec{\omega}_{\perp}$, the component perpendicular to the magnetic field $\vec{\omega}_{\perp} \perp \vec{B}$ is damped and the rigid body asymptotically ends rotating in the direction of the magnetic field $\vec{B}$ (Ormsby, 1967).

This last property of the eddy currents phenomenon can be explained as follows. The vector $\vec{\Omega}$ can be expressed as the sum of three vectors that go along the principal directions of M:

$$\vec{\Omega} = \vec{\Omega}_1 + \vec{\Omega}_2 + \vec{\Omega}_3 = (\vec{\omega}_1 + \vec{\omega}_2 + \vec{\omega}_3) \times \vec{B}. \tag{23}$$

In addition, each $\vec{\omega}_i$ can be split as a component parallel and perpendicular to the magnetic field $\vec{\omega}_i = \vec{\omega}_{||i} + \vec{\omega}_{\perp i}$. In addition, the eddy current torque is the sum of three components due to each $\vec{\Omega}_i$:

$$\vec{T} = (M_1\vec{\Omega}_1 + M_2\vec{\Omega}_2 + M_3\vec{\Omega}_3) \times \vec{B} = \vec{T}_1 + \vec{T}_2 + \vec{T}_3, \tag{24}$$

where M_i are the three eigenvalues of the Magnetic Tensor M. Therefore, each T_i ($i = 1, 2, 3$) will be:

$$\vec{T}_i = M_i \left(\vec{\omega}_i \times \vec{B}\right) \times \vec{B} = -M_i B^2 \vec{\omega}_{\perp i}. \tag{25}$$

All the components of $\vec{\omega}_{\perp i}$ are damped but each one at a different rate. Therefore, asymptotically $\vec{\omega}_{\perp} \to 0$ and consequently, the final angular velocity will be parallel to the magnetic field $\vec{B}$.

3.3. Evaluation of the Magnetic Tensor by F.E.M.

The Laplace Equation (12) with Neumann conditions (13) allows for a Finite Element Method (FEM) solution of the kind:

$$K\Psi - f = 0, \tag{26}$$

where Ψ is a vector that contains all the effective potentials of the N nodes in the FEM ψ_i $(i = 1, ..., N)$, K is the "stiffness" matrix, f the force vector given by Zienkiewicz (Zienkiewicz, 1978). The stiffness matrix and force vector of each element of the FEM has the form:

$$K_{ij}^{(el)} = \sigma \int_{V^{(el)}} (\sum_{k=1}^{3} \frac{\partial N_i^{(el)}}{\partial x_k} \frac{\partial N_j^{(el)}}{\partial x_k}) dV, \tag{27}$$

$$f_i^{(el)} = \sigma \int_{V^{(el)} \cup \partial V} (\vec{j}_{part} \cdot \vec{n}_v) N_i^{(el)} dA, \tag{28}$$

where the superindex (el) denotes an element of the mesh, $V^{(el)}$ is the volume of each element, $N_i^{(el)}$ are the interpolating functions inside each element and $\vec{j}_{part}$ is given by (10). The FEM will give the solution for the scalar function ψ and the current density vector $\vec{j}$ at the Gaussian points of each element:

$$\vec{j}^{(el)}(\vec{r}) = \vec{j}_{part}(\vec{r}) - \sigma \sum_{i=1}^{n} \psi_i^{(el)} \frac{\partial N_i^{(el)}}{\partial \vec{r}}(\vec{r}) \quad \forall \vec{r} \in V^{(el)}, \tag{29}$$

where the sum is for the n nodes of the generic element $V^{(el)}$.

The dissipated energy transforms into heat as a result of Joules Law (Landau & Lifshitz, 1984):

$$-\dot{E} = \int \frac{j^2}{\sigma} dV = \vec{\Omega}^t M \vec{\Omega}, \tag{30}$$

where the linear dependence on $\vec{\Omega}$ of the calculated $\vec{j}$ provides us with the postulated quadratic form for $\dot{E}$. It gives also a practical way for computing M.

First, solve the FEM for the three cases $\vec{\Omega}^{(1)} = \begin{bmatrix} 1 \\ 0 \\ 0 \end{bmatrix}$, $\vec{\Omega}^{(2)} = \begin{bmatrix} 0 \\ 1 \\ 0 \end{bmatrix}$, $\vec{\Omega}^{(3)} = \begin{bmatrix} 0 \\ 0 \\ 1 \end{bmatrix}$ and save the corresponding $\vec{j}^{(k)}(\vec{r})$ $(1 \leq k \leq 3)$ for the Gaussian points of all the elements.

Thanks to the linearity of the solution with $\vec{\Omega}$ for a given $\vec{\Omega} = \begin{bmatrix} \Omega_1 \\ \Omega_2 \\ \Omega_3 \end{bmatrix} = \sum_{i=1}^{n} \Omega_i \vec{\Omega}^{(i)}$, the solution for $\vec{j}$ can be expressed as (16).

Introducing Equation (16) in (30), M can be computed by numerical Gaussian integration for all the elements.

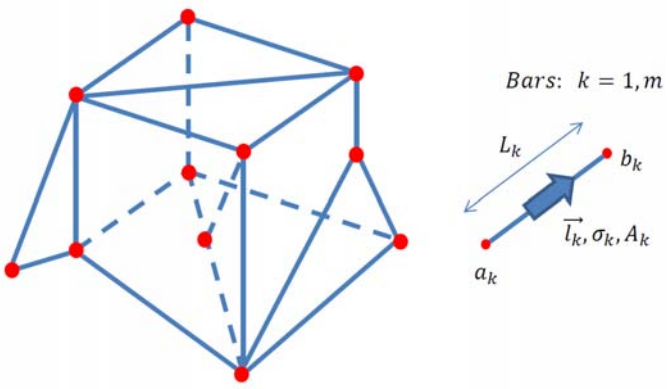

Figure 1: FEM based on bars (Frame model).

$$M_{kl} = \sum_{(el)} \int_{V^{(el)}} \frac{\vec{j}^{(k)} \cdot \vec{j}^{(l)}}{\sigma} dV. \tag{31}$$

3.3.1. The approximate Frame Model.

The Frame Model can be seen as the simplest FEM model for the previously defined problem. This model allows for a clear comprehension of the eddy currents phenomenon and for the derivation of some explicit formulae from which new concepts are developed (e.g. the Magnetic Tensor).

First the rigid body must be divided into m bars and n nodes (see Figure 1) where each bar has a length L_k, a conductivity σ_k and a cross section A_k. A constitutive constant is assigned to each bar $D_k = \frac{\sigma_k A_k}{L_k}$. The subindex k denotes the number of the bar $(k = 1, ..., m)$.

Each bar has a local coordinate l and a unit vector $\vec{l}_k = \frac{\vec{L}_k}{L_k}$. The position of the center of gravity of the bar is given by the position vector $\vec{r}_k$. The electric intensity of each bar $J_k = A_k \cdot j_k$ is defined as the product of the electric current density j_k and its cross section A_k. The electric intensities of the m bars can be grouped in one vector as:

$$J = \begin{bmatrix} J_1 \\ \vdots \\ J_m \end{bmatrix}. \tag{32}$$

A scalar function ψ_i (effective potential) is assigned to each node $(i = 1, ..., n)$. ψ_i is a potential function that is defined except for a constant which can be arbitrarily assigned to one of the nodes. The function is set to zero at node n and they can also be grouped in one vector Ψ:

$$\Psi = \begin{bmatrix} \psi_1 \\ \vdots \\ \psi_{n-1} \\ 0 \end{bmatrix}. \tag{33}$$

Using the particular solution (10) for the current density vector, the general solution (34) for the current density vector is adopted,

$$\vec{j} = \frac{\sigma}{2}(\vec{\Omega} \times \vec{r}) - \sigma \nabla \psi. \tag{34}$$

The boundary condition (4) allows for the current density vector to be projected in the direction of each bar so that the current stays inside its volume. Therefore, the module of the current density for each bar is:

$$j_k = \vec{j}_k \cdot \vec{l}_k = (\frac{\sigma_k}{2}(\vec{\Omega} \times \vec{r}) - \sigma_k \cdot \nabla \psi(\vec{r})) \cdot \vec{l}_k. \tag{35}$$

Since $j_k = \frac{J_k}{A_k}$ is constant along the bar, the previous expression can be easily integrated along the length of each bar, giving:

$$J_k = D_k(\frac{1}{2}(\vec{r}_k \times \vec{L}_k) \cdot \vec{\Omega} - \Delta\psi_k). \tag{36}$$

The term $\Delta\psi_k = \psi_{bk} - \psi_{ak}$ is the effective potential difference between the nodes a_k and b_k of bar k. A new parameter is defined for each bar $\vec{S}_k = \vec{r}_k \times \vec{L}_k$ and Equation (36) can be expressed in a matricial way for all the bars:

$$J = D(\frac{1}{2}S \cdot \vec{\Omega} - \Delta\Psi). \tag{37}$$

J is a vector of dimensions $(m \times 1)$ that contains the intensities of each bar, $D = diag(D_k)$ is a diagonal matrix of dimensions $(m \times m)$ that contains the constitutive constants for each bar, S is a matrix of dimensions $(m \times 3)$ that contains the cross products $\vec{r}_k \times \vec{L}_k$ for each bar and $\Delta\Psi$ is a vector of dimensions $(m \times 1)$ which contains the effective potential difference for each bar. J, $\Delta\Psi$ and Ψ are unknown variables.

Now the continuity equation in all the nodes is imposed. This linear system of n equations (one for each node) and m unknown variables (the electric intensity for each bar J_k) can be expressed as shown in (38) using a matrix H that links all the bars. Equation (39) gives $\Delta\Psi$ as a function of Ψ.

$$H \cdot J = 0, \tag{38}$$

$$\Delta\Psi = -H^t\Psi \tag{39}$$

Combining Equations (37, 38, 39), the solution for the current intensities of the bars is found:

$$J = \frac{1}{2}(I - DF)DS\vec{\Omega}, \tag{40}$$

where I is the identity matrix of dimensions $(m \times m)$ and F is a symmetric matrix defined as:

$$F = H^t(K)^{-1}H = H^t(HDH^t)^{-1}H = F^t. \tag{41}$$

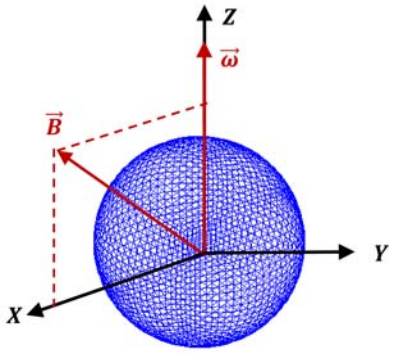

Figure 2: Spherical Shell grid.

It must be noted that $K = HDH^t$ is a singular matrix and therefore, K^{-1} must be seen as an appropriate pseudoinverse. As the scalar function ψ was assigned zero for node n, matrix K can be reduced to K_{red} by removing the last row and column of the matrix and then compute the inverse of K_{red}. The pseudo-inverse of K will be taken as the inverse of K_{red} with an additional last row and column of zeros.

Finally, the heat dissipated by all the bars due to Joule's effect is:

$$\vec{\Omega}^t M \vec{\Omega} = \sum_{k=1}^{m} \frac{J_k^2}{D_k} = J^t D^{-1} J, \tag{42}$$

and the Magnetic Tensor is deduced from Equation (42) which has the final explicit expression

$$M = \frac{1}{4}S^t D(I - FD)D^{-1}(I - DF)DS. \tag{43}$$

3.4. Analytical solutions of the Magnetic Tensor and validation of the Frame Model.

Smith (Smith, 1962) and Ormsby (Ormsby, 1967) give several analytical solutions of the eddy current torque for certain canonical shapes and specific orientations of the angular velocity vector $\vec{\omega}$ and the magnetic field $\vec{B}$. These solutions are used to validate the frame model.

3.4.1. Spherical Shell.

The analytical solution of the eddy current torque induced on a spherical shell is (Ormsby, 1967):

$$\vec{T} = \frac{2\pi}{3}\sigma R^4 e(\vec{\omega} \times \vec{B}) \times \vec{B}. \tag{44}$$

where R is the radius of the spherical shell, e is its thickness and σ the electrical conductivity. A frame model is used to design the spherical shell as shown in Figure 2.

The torque on the spherical shell is evaluated numerically using the frame model for the following data:

- $\vec{\omega} = [0, 0, 50]$ deg/sec
- $\vec{B} = [150, 0, 150]$ μT

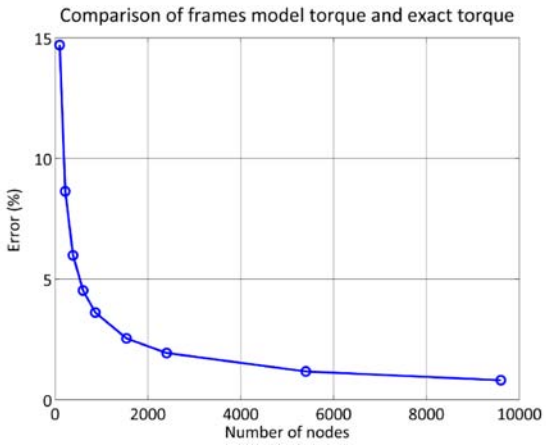

Figure 3: Error (%) of the torque obtained with the Frame Model with respect to the analytical solution for a spherical shell.

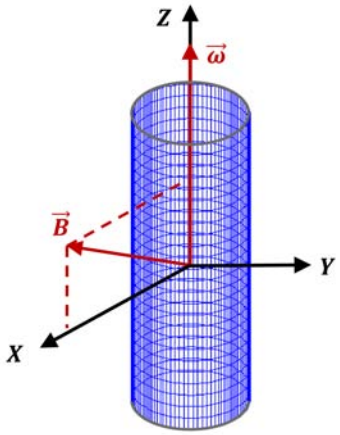

Figure 4: Cylindrical Shell grid.

- $R = 2$ m
- $e = 0.001$ m
- $\sigma = 35000000$ S/m

Figure 3 shows the difference between the torque evaluated using the Frame Model and the analytical solution given by Orsmby (Ormsby, 1967). As the number of nodes is increased, the numerical model becomes more accurate.

The analytical solution of the Magnetic Tensor for a spherical shell has the form:

$$M = \frac{2\pi}{3}\sigma R^4 e \begin{bmatrix} 1 & 0 & 0 \\ 0 & 1 & 0 \\ 0 & 0 & 1 \end{bmatrix}. \quad (45)$$

3.4.2. Open cylindrical shell

Smith (Smith, 1962) published the analytical solution in 1962 of the eddy current torque induced on a cylindrical shell without covers that is rotating about its axis of symmetry. The cylinder is assumed to be rotating about the Z axis with a rotational speed $\vec{\omega} = \omega\vec{k}$ and it is subject to a magnetic field $\vec{B} = B_x\vec{i} + B_z\vec{k}$. The analytical expression of the torque given by Smith, for this particular case, is:

$$\vec{T} = \pi\sigma B_x \omega R^3 eL(1 - \frac{2R}{L}tanh(\frac{L}{2R}))(B_x\vec{i} - B_z\vec{k}), \quad (46)$$

where R is the radius of the cylinder, L is its length, e is its thickness and σ the electrical conductivity. A frame model is used to design the cylindrical shell as shown in Figure 4, where the Z axis is the axis of symmetry of the cylinder.

The torque on the cylindrical shell is evaluated numerically using the frame model for the following data:

- $\vec{\omega} = [0, 0, 50]$ deg/sec
- $\vec{B} = [150, 0, 50]$ μT

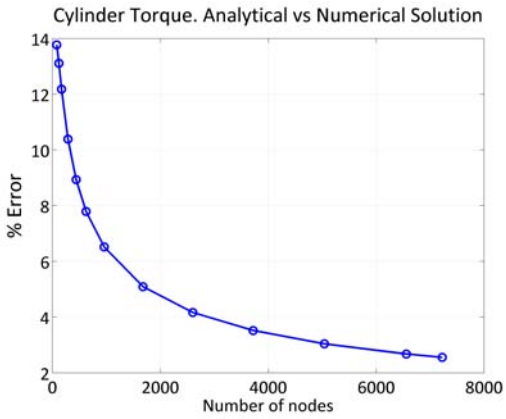

Figure 5: Error (%) of the torque obtained with the Frame Model with respect to the analytical solution for a cylindrical shell.

- $R = 1.33$ m
- $L = 7.372$ m
- $e = 0.001$ m
- $\sigma = 35000000$ S/m

Figure 5 shows the difference between the torques evaluated using the Frame Model and the analytical solution given by Smith (Smith, 1962). As the number of nodes is increased, the numerical model becomes more accurate.

The analytical solution of the Magnetic Tensor for a open cylindrical shell with its axis of symmetry parallel to the Z axis has the form:

$$M = \pi\sigma R^3 eL \begin{bmatrix} \gamma & 0 & 0 \\ 0 & \gamma & 0 \\ 0 & 0 & \frac{1}{2} \end{bmatrix}, \quad (47)$$

where $\gamma = 1 - \frac{2R}{L}tanh\frac{L}{2R}$. The components M_{11} and M_{22} are based on the formula (46) given by Smith while M_{33} is obtained below analytically. Expression (47) generalises the solution given by Smith and it enables the torque

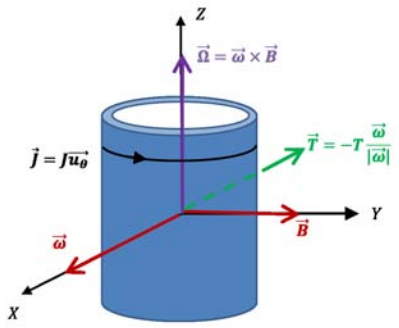

Figure 6: Open cylindrical shell rotating along an axis perpendicular to the axis of symmetry.

to be evaluated for any given direction of the angular velocity vector and the magnetic field.

In order to evaluate M_{33}, the particular solution (10) is used to solve Equations (2, 3, 4) for the configuration shown in Figure (6).

In this case, the particular solution $\vec{j}_{part}$ is $\vec{j} = j_\theta \vec{u}_\theta = \frac{\sigma}{2}\Omega r \vec{u}_\theta$. This leads to the following Laplace equation in ψ with homogeneous Neumann boundary conditions,

$$\nabla^2 \psi = 0 \ \ \forall P \in V, \tag{48}$$

$$\frac{\partial \psi}{\partial n_v} = 0 \ \ \forall P \in \partial V, \tag{49}$$

which has the solution $\psi = constant$ (Weinberger, 1995). Then, taking into account that the thickness of the cylindrical wall is very small ($e << r$), the current intensity vector can be expressed as $j_\theta = \frac{\sigma}{2}\Omega R$. Now, in order to evaluate M_{33}, Equation (31) is employed with $\vec{\Omega}^{(3)} = \begin{bmatrix} 0 \\ 0 \\ 1 \end{bmatrix}$ and $\vec{j}^{(3)} = \frac{\sigma}{2} R \vec{u}_\theta$:

$$M_{33} = \int_V \frac{\vec{j}^{(3)} \cdot \vec{j}^{(3)}}{\sigma} dV = \left(\frac{\sigma R}{2}\right)^2 \frac{V}{\sigma} = \frac{\pi}{2}\sigma R^3 e L. \tag{50}$$

3.4.3. Flat Plates

The eddy current torque induced on a circular flat plate can be computed analytically using perturbations theory. Cylindrical coordinates (ρ, θ, z) are used to locate a generic point of the flat plate (see Figure 7). This plate is assumed to have a conductivity σ, a thickness e, an external radius a and an internal radius b.

The particular solution (10) is used,

$$\vec{j}_{part} = \frac{\sigma}{2}\vec{\Omega} \times \vec{r} = \frac{\sigma}{2}\Omega \vec{n}_l \times (\rho \vec{u}_\rho + z\vec{k}) = \frac{\sigma\Omega}{2}(z n_{l\theta}\vec{u}_\rho + (\rho n_{lz} - z n_{l\rho})\vec{u}_\theta - \rho n_{l\theta}\vec{k}), \tag{51}$$

where the vector $\vec{n}_l$ is defined as:

$$\vec{n}_l = \vec{\Omega} / \left|\vec{\Omega}\right| = n_{l\rho}\vec{u}_\rho + n_{l\theta}\vec{u}_\theta + n_{lz}\vec{k}. \tag{52}$$

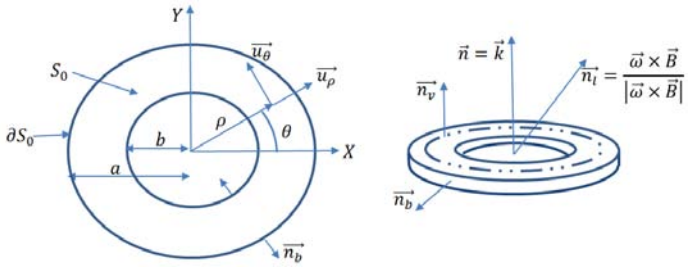

Figure 7: Cylindrical coordinates and normal vectors to the circular flat plate.

As explained in Section (3.1), this particular solution leads to the Laplace Equation (12) with Neumann boundary (13) conditions for the scalar function ψ. The solution of the Laplace equation can be expressed as (53), assuming that the coordinate $z \to 0$.

$$\psi(\rho, \theta, z) = \psi_0(\rho, \theta) + z\psi_1(\rho, \theta) + ... \tag{53}$$

Neglecting the terms of order $o(z^2)$, the following Laplace equation is reached:

$$\nabla\psi^2 = \frac{1}{\rho}\frac{\partial}{\partial\rho}\left(\rho\frac{\partial\psi}{\partial\rho}\right) + \frac{1}{\rho^2}\frac{\partial^2\psi}{\partial\theta^2} + \frac{\partial^2\psi}{\partial z^2} = \nabla_{\rho\theta}\psi_0 + z\nabla_{\rho\theta}\psi_1 = 0. \tag{54}$$

Now, the boundary conditions are imposed. At $z = \pm\frac{e}{2}$, $\vec{j} \cdot \vec{k} = 0$, therefore:

$$\begin{gathered} \mp\psi_1 \pm \frac{\sigma\Omega}{2}(\vec{n}_l \times \vec{r}) \cdot \vec{k} = 0 \to \\ \to \mp\psi_1 \mp \frac{\sigma\Omega}{2}\vec{n}_l \cdot \rho\vec{u}_\theta = 0 \to \psi_1 = -\frac{\Omega\rho}{2}n_{l\theta}. \end{gathered} \tag{55}$$

Consequently, up to first order infinitesimal terms, ψ is equal to:

$$\psi = \psi(\rho, \theta, z) = \psi_0(\rho, \theta) - z\frac{\Omega\rho}{2}n_{l\theta} \tag{56}$$

and $\vec{j}$ is equal to:

$$\vec{j} = -\sigma\frac{\partial\psi_0}{\partial\rho}\vec{u}_\rho + \sigma\left[-\frac{1}{\rho}\frac{\partial\psi_0}{\partial\theta} + \frac{\Omega}{2}(\rho n_{lz} - z n_{l\rho})\right]\vec{u}_\theta. \tag{57}$$

At $\rho = a, b$, $\vec{j} \cdot \vec{u}_\rho = 0$, which leads to the following boundary condition for ψ_0:

$$\frac{\partial\psi_0}{\partial\rho} = 0 \quad at\ \rho = a, b. \tag{58}$$

Equation (54) results in the following equation for ψ_0:

$$\left(\frac{\partial^2}{\partial\rho^2} + \frac{1}{\rho}\frac{\partial}{\partial\rho} + \frac{1}{\rho^2}\frac{\partial^2}{\partial\theta^2} + \frac{\partial^2}{\partial z^2}\right)\left[\psi_0(\rho, \theta) - \frac{z\rho}{2}\Omega n_{l\theta}\right] = 0. \tag{59}$$

Since $n_{l\theta} = -n_{lx}\sin\theta + n_{ly}\cos\theta$ is dependent on θ, Equation (59) reduces to the bidimensional Laplace equation in ψ_0 with homogeneous Neumann boundary conditions:

$$\frac{\partial^2\psi_0}{\partial\rho^2} + \frac{1}{\rho}\frac{\partial\psi_0}{\partial\rho} + \frac{1}{\rho^2}\frac{\partial^2\psi_0}{\partial\theta^2} = 0, \tag{60}$$

$$\frac{\partial\psi_0}{\partial\rho} = 0 \quad for\ \rho = a, b. \tag{61}$$

The solution for (60, 61) is $\psi_0 = constant$ (Weinberger, 1995). Therefore, the complete function ψ is:

$$\psi = \psi(\rho,\theta,z) = constant - z\frac{\lambda\rho}{2}n_{l\theta}. \tag{62}$$

Using the solution obtained for ψ, the electric current density vector can be easily computed as follows:

$$\vec{j} = \frac{\sigma\Omega}{2}\vec{n}_l \times \vec{r} - \sigma\nabla(\psi) = \frac{\sigma\Omega}{2}[2zn_{l\theta}\vec{u}_\rho + (\rho n_{lz} - 2zn_{l\rho})\vec{u}_\theta]. \tag{63}$$

Taking into account that $z \to 0$, the solution reached for the current density vector, up to first order terms, for a the circular flat plate is,

$$\vec{j} = \frac{\sigma}{2}(\vec{\Omega}\cdot\vec{n})\rho\vec{u}_\theta, \tag{64}$$

and the torque for the circular flat plate can be obtained as:

$$\vec{T} = \int \vec{r}\times(\vec{j}\times\vec{B})dV = \sigma\frac{\pi R^4 e}{8}(\vec{\Omega}\cdot\vec{n})\cdot(\vec{n}\times\vec{B}). \tag{65}$$

The Magnetic Tensor for a circular flat plate is derived from the torque:

$$M = \sigma\frac{\pi R^4 e}{8}\begin{bmatrix}0&0&0\\0&0&0\\0&0&1\end{bmatrix} = \sigma\frac{\pi R^4 e}{8}\vec{n}\cdot\vec{n}^T, \tag{66}$$

It can be easily verified that the preceding mathematical development shows a clear similarity with the Saint Venant torsion theory for beams (Timoshenko, 1934). As a result of this, the Magnetic Tensor can be easily generalised for other geometries by introducing a constant inherent to the specific geometry of the plate C_T. This constant corresponds to the torsional rigidity of St Venant. The Saint Venant torsion theory of beams is governed by a Laplace equation with Neumann boundary conditions, where the boundary conditions only differ in a constant factor from our Equations (12,13) (Timoshenko, 1934). By comparing the exact solution of Saint Venant theory for a beam of circular section and our circular flat plate, a factor $e/4$ needs to be introduced in our solution for the Magnetic Tensor. Finally, the general solution of the Magnetic Tensor for a flat plate can be expressed as:

$$M = \frac{1}{4}\sigma e C_T \vec{n}\cdot\vec{n}^T, \tag{67}$$

Figure 8 gives the C_T constants computed for different flat plate shapes (Timoshenko, 1934).

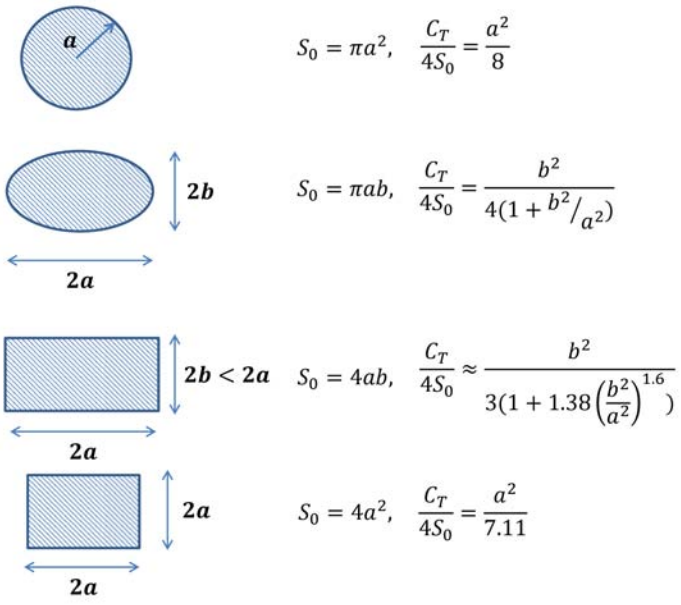

Figure 8: Flat Plates constants to evaluate the Magnetic Tensor.

4. Active De-Tumbling Method based on Eddy Currents

Natural rotation damping due to the Earth's magnetic field has been observed in LEO orbits for certain spacecraft (Yu, 1963; Williams & Meadows, 1978; Boehnhardt et al., 1989). The idea presented here is to subject a space debris object to an enhanced magnetic field to damp its rotation and allow for its capture and subsequent de-orbiting phase. The braking method has the advantage that it requires no mechanical contact with the target object.

4.1. De-tumbling Design

The de-tumbling will be carried out actively from a chaser spacecraft that has one or more electromagnetic coils (see Figure 9). The coil will be pointed towards the target in different directions so that all its rotational velocity components are damped. In order to avoid electromagnetic interferences on the instruments of the chaser, two solutions are proposed. A deployable structure can be used with the electromagnetic coil at its end in order to generate the magnetic field at a certain distance from the chaser module. The second option consists on shielding the sensitive instruments on the chaser with ferromagnetic material such as a mu-metal alloy which has been employed in past missions (NASA, 1970).

In order to achieve a reasonable value of de-tumbling time, as well as low mass, power and volume for the electromagnetic coil on the chaser spacecraft, a coil based on high temperature superconducting (HTS) wires is baselined. Superconductors have evolved enormously since their discovery in 1911. HTS wires have a standard working temperature of 77 K which facilitates their use in space as no excessive cooling is needed (Yuan, 2011).

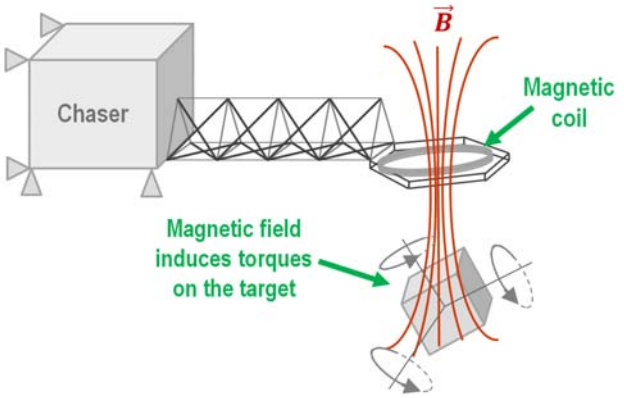

Figure 9: Design 1 of the Active de-tumbling method.

The first analysis of the de-tumbling process (Sections 4.3, 4.4, 4.5) assumes a constant and homogenous magnetic field ($\vec{B}(\vec{r},t) = constant$) which gives a first approximate solution to the problem. However, it would be impractical to design a de-tumbling system that pursues the generation of a homogeneous magnetic field due to high mass and volume requirements for the coil. In order to achieve a homogeneous field, a Helmholtz-like coil could be designed. This would require a chaser spacecraft with two magnetic coils or two different chaser spacecrafts with separate magnetic coils so that the two coils are placed on each side of the space debris object with both magnetic moments pointing in the same direction. However, in order to achieve a homogeneous magnetic field, the distance between the two coils needs to be equal to the radius of the coils (Vanderlinde, 2004). For an Ariane Upper Stage H10 target which has a total length of 11 meters, two coils of at least 22 meters would be required. This design is impractical due to the volume and mass required by the coils as well as the duplication of the subsystems.

A second interesting option would be to place the target object at the center of one coil because this is the point where the magnetic field is strongest. For an Ariane Upper Stage H10 target, a coil of at least 11 meters in diameter is necessary. This size exceeds the diameter of existing space launch systems and a deployable magnetic coil would be necessary. Some studies on deployable HTS magnetic coils have been carried out for human space applications but the Technology Readiness Level is still very low (NASA, 2012; Battison, 2013).

Taking into account the existing technology on HTS coils, the most simple design consists on a fixed-size coil which can cope with the maximum available diameter of current space launchers (4 meters diameter for an Ariane-5 launcher (Arianespace , 2011)). The coil would be placed at a certain distance from the space debris object as shown in Figure 9. This will inevitably generate a non- homogeneous magnetic field. Section (4.6) presents some considerations on the consequences of having a spatial gradient in the magnetic field. It is shown that a reduction in the eddy currents torque of approximately $5-10\%$ takes place for relative distances of 5 meters between the coil and the target surface for the studied case. Therefore, the theory developed in Section 3 can be applied introducing an efficiency factor in the eddy currents torque.

4.2. Dynamics Chaser-Target

Assuming, as a first approximation, that the dynamics chaser-target can be treated as an isolated system, the conservation of momentum and angular momentum can be used.

- Conservation of momentum: The sum of the resultant forces acting on chaser and target is equal to zero, $\vec{f}_t + \vec{f}_c = \vec{0}$. Due to the spatial gradient of the magnetic field, a force $\vec{f}_t$ will appear on the target object, and taking into account the conservation of momentum, the same force with opposite direction will appear on the target ($\vec{f}_c = -\vec{f}_t$). The chaser spacecraft will need to correct its relative position in order to maintain a constant distance with respect to the target object. If the magnetic field were homogeneous and constant, no forces would appear on the system chaser-target (see Section(4.6)).

- Conservation of angular momentum: The sum of the resultant torques acting on the system is equal to zero. Given the fact that the resultant of forces is equal to zero, the sum of torques can be expressed at an arbitrary point. At O_c (the point of force application at the chaser),

$$\vec{0} = \vec{T}_t + \vec{T}_c + \vec{r}_{ct} \times \vec{f}_t \rightarrow \vec{T}_c = -\vec{T}_t - \vec{r}_{ct} \times \vec{f}_t, \quad (68)$$

  where $\vec{r}_{ct}$ is the position vector of the COG of the conductive mass of the target with respect to O_c.

  In the absence of forces on the system (no spatial gradient of the magnetic field), the chaser will receive the same torque with opposite direction as the one induced on the target object due to the eddy currents phenomenon $\vec{T}_c = -\vec{T}_t$. This torque will need to be counteracted on the chaser spacecraft so that the magnetic coil always points in the right direction. Therefore, the de-tumbling process can be described as a *'Contactless Manoeuvre'*.

In reality, additional external perturbations need to be incorporated in the dynamics chaser-target such as orbital perturbations (e.g. Earth's magnetic field, Earth's gravity gradient, etc.) or the presence of ferromagnetic material on the objects. These perturbations need to be counteracted by the chaser spacecraft in order to maintain a constant relative distance with respect to the target object and the correct pointing of the magnetic coil towards the target.

The main magnetic moment on the chaser spacecraft is given by the electromagnetic coil on-board shown in Equation (69),

$$m_c = NIA, \tag{69}$$

where N is the number of turns, $A = \pi R_{coil}^2$ is the area of the coil and I is the intensity. The general expression of the torque (14) applied to the chaser object, leads to Equation (70),

$$\vec{T}_c = \vec{m}_c \times \left(\vec{B}_{target} + \vec{B}_{Earth}\right), \tag{70}$$

where $\vec{B}_{target}$ is the magnetic field generated by the target object due to the induced magnetic moment caused by the eddy currents and $\vec{B}_{Earth}$ is the magnetic field of the Earth.

Due to the fact that the magnetic moment $\vec{m}_c$ in (69) does not depend on the magnetic field vector, Equation (70) shows that the two effects considered on the torque are linear in $\vec{B}$. Therefore, the principle of superposition can be used and each effect can be treated separately.

As an example, these torques have been evaluated for an electromagnetic coil of 2 meters of radius, 500 turns and 80 amperes, which is below the critical intensity for a HTS wire working at 77 K (Yuan, 2011). The target object is a spherical shell of 2 meters of radius made of aluminium and a thickness of 1 mm which is rotating at 50 deg/sec. In addition, the relative distance between the coil and the COG of the target object is assumed to be 10 meters. In this example, the maximum torque is evaluated, that is, the magnetic moment of the chaser spacecraft is assumed to be perpendicular to the magnetic field vector. The maximum torque induced by the target is:

$$\vec{T}_{1c} = \vec{m}_c \times \vec{B}_{target} = 0.0092\ \mathrm{N \cdot m}, \tag{71}$$

The torques due to both effects are depicted in Figure 10 for different altitudes. The torque due to the Earth's magnetic field outcomes the torque due to the interaction chaser-target by several orders of magnitude for low Earth orbits. Therefore, in this example, the torque induced by the target object can be neglected. In order to counteract the torque induced by the Earth's magnetic field, a control moment gyro (CMG) can be used on the chaser spacecraft including an external actuator torque to desaturate the CMG when necessary (Votel, 2012) .

4.3. Characteristic Time of Decay

Introducing the eddy current torque into Euler equations, the following equation is obtained:

$$I\dot{\vec{\omega}} + \vec{\omega} \times I\vec{\omega} = M(\vec{\omega} \times \vec{B}) \times \vec{B}, \tag{72}$$

In the case of a spherical shell, both I and M are diagonal tensors and the term $\vec{\omega} \times I\vec{\omega}$ is zero. Therefore, Equation (72) is simplified to the following:

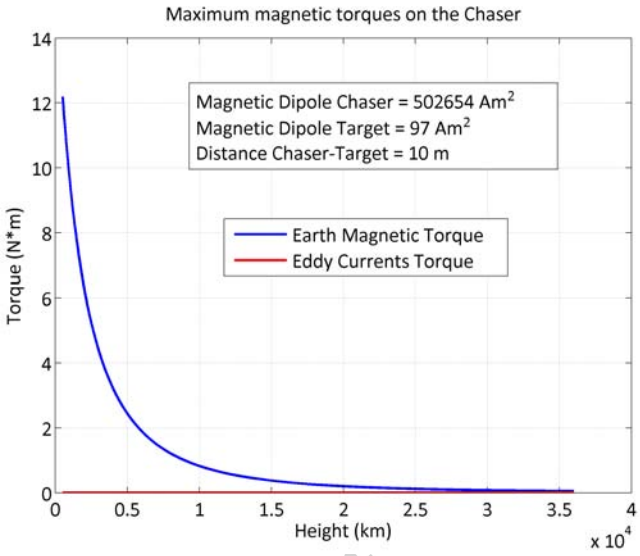

Figure 10: Maximum magnetic fields on the chaser objects caused by the Earth's magnetic field and the target object for a given geometry of the coil and the target object.

$$\dot{\omega}_\perp + \frac{\omega_\perp}{\tau} = 0, \tag{73}$$

where $\omega_\perp$ is the perpendicular component of the angular velocity with respect to the magnetic field. Consequently, only the perpendicular component of the rotational speed is damped and this component has an exponential decay with a characteristic time of decay τ equal to:

$$\tau_i = \frac{I_i}{M_i B^2} \quad I_1 = I_2 = I_3,\ M_1 = M_2 = M_3. \tag{74}$$

In Equation (73), I_i and M_i are the principal components of the inertia tensor and magnetic tensor respectively. In general, the principal directions of the inertia tensor and the magnetic tensor will not coincide for a non-spherical body. Hence, Equation (72) can not always be simplified, making it necessary to integrate Euler equations numerically. As it was proved by Equation (25), the rate of decay will be, in general, different for each component of $\vec{\omega}_\perp$ along the principal axes of M.

Nonetheless, expression (74) gives some qualitative information of this process. The characteristic time of decay is inversely proportional to the square of the magnetic field. Consequently, the magnitude of the magnetic field plays an important role on the braking time. In addition, the ratio of conductive material versus non-conductive material is related to the ratio $\frac{I_i}{M_i}$ and therefore, the more conductive material is present in the body, the lower the characteristic time of decay is.

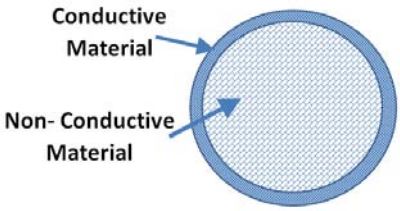

Figure 11: Metallic spherical shell filled with non-conductive material.

4.4. Spherical Shell Analysis

Euler equations can be integrated analytically in the case of a metallic spherical shell. For this particular case, the characteristic time of decay is:

$$\tau = \frac{I_i}{\frac{2\pi}{3}\sigma R^4 e B^2} \tag{75}$$

and the evolution of $\omega_\perp$ with time is:

$$\omega_\perp = \omega_{\perp 0} \cdot exp(-\frac{t}{\tau}). \tag{76}$$

It is now assumed that the conductive mass is located at the surface of the sphere (simulating a thin metallic structure) and the inside is made of non-conductive material (see Figure 11).

The characteristic time of decay is shown in Equation (77) as a function of the conductive versus non-conductive material. The subindex c stands for conductive material and the subindex nc stands for non-conductive material. In the formula it is assumed that the thickness of the spherical shell is small compared to the radius of the shell and therefore $R_c \approx R_{nc}$. The parameter m is the mass and ρ is the density of the material.

$$\tau = \frac{I_c + I_{nc}}{\frac{2\pi}{3}\sigma R_c^4 e_c B^2} = \frac{\frac{2\pi}{3} m_c R_c^2 + \frac{2\pi}{3} m_{nc} R_{nc}^2}{\frac{2\pi}{3}\sigma R_c^4 e_c B^2} \approx \approx \frac{4\rho_c}{\sigma B^2}(1 + \frac{3}{5}\frac{m_{nc}}{m_c}). \tag{77}$$

It must be noted that the characteristic time of decay does not depend on the dimensions of the object. Figure 12 shows the characteristic time of decay versus the percentage of non-conductive mass for a sphere which has a thin aluminum metallic core and is subjected to 150 μT of magnetic field. For a 10% of conductive material versus total mass, the characteristic time of decay is 1 day.

4.4.1. Precession of the axis of rotation

This phenomenon is caused when there is a component of the angular velocity vector parallel to the magnetic field. This component is not damped and it will consequently cause a precession of the axis of rotation of the object.

In order to visualise this effect a fully conductive spherical shell is considered with the following characteristics:

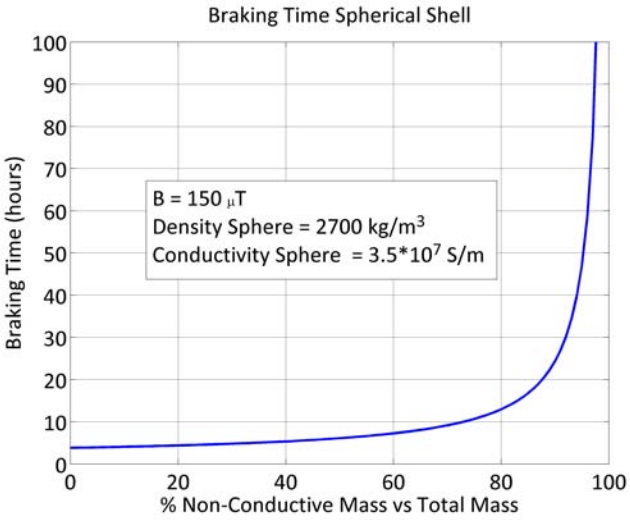

Figure 12: Characteristic time of decay for a spherical shell for different ratios of conductive material.

- $\vec{\omega} = [0, 0, 50]$ deg/sec
- $\vec{B} = [150, 0, 150]$ μT
- Radius $R = 2$ m
- Thickness $e = 0.001$ m
- Conductivity $\sigma = 35000000$ S/m

Figures 13 and 14 show the evolution of the angular velocity vector in the body and inertial reference frames respectively. Only the component of the angular velocity perpendicular to the magnetic field is damped and the final direction of the rotational speed must be parallel to the magnetic field vector. In the example analyzed, the magnetic field and the angular velocity vectors initially form an angle of 45 degrees. Therefore, the angular velocity asymptotically decreases in a factor of $\frac{\sqrt{2}}{2}$.

This results in a decay of the rotational speed from $\omega_0 = 50$ deg/s to $\omega_f = \frac{\sqrt{2}}{2}50 = 35.4$ deg/s as shown in Figure 13. Figure 14 shows that the final angular velocity vector is parallel to the magnetic field. In addition, Figure 15 depicts the initial and final moments of the simulation in order to visualise this phenomenon.

In order to damp all the components of a space debris object during the de-tumbling process, the chaser may need to change the relative position of the electromagnetic coil with respect to the target.

4.5. Case Study: Ariane H10 Upper Stage

Suitable targets for the eddy currents de-tumbling method are upper stages due to their high ratio of conductive material. Here, a case study is presented for an Ariane H10 upper stage in a LEO orbit. There are currently several of these space debris objects in high inclination LEO orbits (N2YO Webpage, 1989).

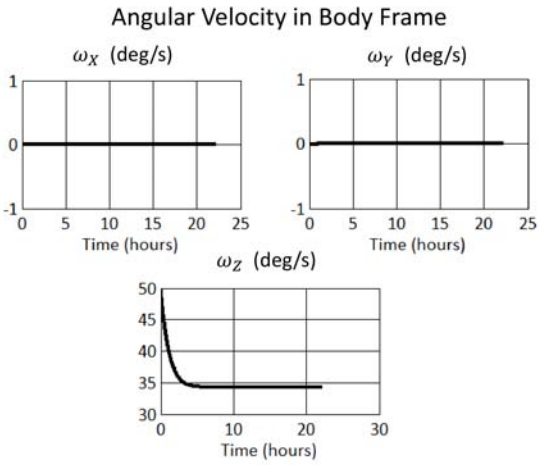

Figure 13: Evolution of the rotational velocity in the body reference frame.

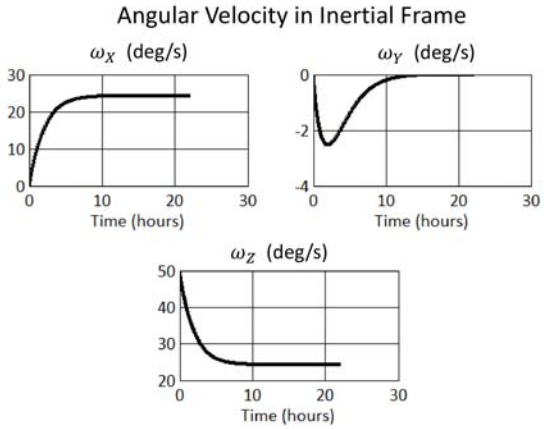

Figure 14: Evolution of the rotational velocity in the inertial reference frame.

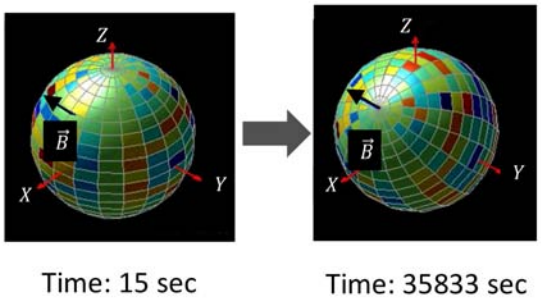

Figure 15: Precession of the axis of rotation of a conductive rotating spherical shell.

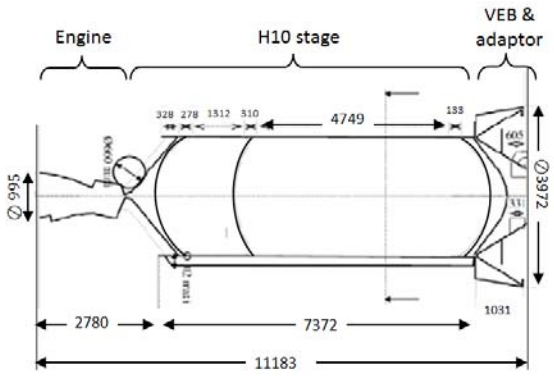

Figure 16: Ariane 4 H10 Upper Stage dimensions in mm.

The dimensions of this object (see Figure 16), total mass, center of gravity and inertia tensor were provided by Centre National d'Etudes Spatiales (CNES). The total mass of the object including the Vehicle Equipment Bay (VEB) and adaptor is 2154 kg. The rocket body consists of three main parts. First of all, there is the engine HM-7B. The central part is the H10 stage which has two propellant tanks (oxygen and hydrogen tanks). The structure consists of a cylinder with two hemispherical bulkheads which has a diameter of 2600 mm and length 7372. Its total dry mass is 700 kg and they are entirely made of aluminium alloy 7020 (Arianespace , 1999). The third part is the VEB and adaptor. In this part, the main instruments that control the launcher are located. Its structure is made of CFRP panels and an aluminum platform (Arianespace , 1999; ECSS, 2011).

The inertia matrix of the object is:

$$I_{H10} = \begin{bmatrix} 28000 & 0 & 0 \\ 0 & 28000 & 0 \\ 0 & 0 & 3000 \end{bmatrix} \text{ kg} \cdot \text{m}^2. \qquad (78)$$

In order to obtain the magnetic tensor of this object, the conductive material that was taken into account is the aluminum tanks of the H10 stage. A Frame Model was developed as seen in Figure 17. Therefore the ratio of conductive material versus total mass considered for this object is 32.5%. This value will probably be conservative as both the engine and VEB may contain metallic parts. The number of nodes used in the Frame Model is 7778. A F.E.M. of an open cylinder of similar size and the same number of nodes was analysed in Section 3.4.2 and the number of nodes used corresponds to an error of 2.7% in the frame model of a cylinder (see Figure 5). This comparison gives an order of magnitude of the precision of the method employed in this analysis.

The magnetic tensor obtained for this object is:

$$M_{H10} = \begin{bmatrix} 5.908 & 0 & 0 \\ 0 & 5.908 & 0 \\ 0 & 0 & 1.951 \end{bmatrix} \cdot 10^6 \text{ S} \cdot \text{m}^4. \qquad (79)$$

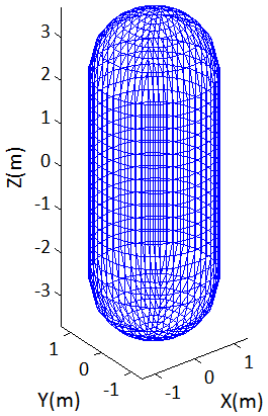

Figure 17: Frame Model for Ariane 4 H10 metallic structure.

Due to the cylindrical symmetry of the object, both the inertia tensor and the magnetic tensor are diagonal in the reference frame adopted. Hence, no cross terms appear in both matrices.

The expected rotational speed of these objects may vary greatly. Papushev et al. (Papushev et al., 2009) published a detailed paper in 2009 on the rotation rates measured with optical measurements for geostationary satellites. The rotation speed varies from 0.8 deg/sec up to 180 deg/sec. The work published by Praly et al. (Praly et al., 2012) on Ariane upper stages state that the expected rotational rates lie between 37.5 deg/sec and 60 deg/sec.

The analysed object is placed on a circular orbit of 760 km where the main perturbation that affects its rotational motion is the gravity gradient. The initial rotational speed considered is $\vec{\omega} = [28.8, 28.8, 28.8]$ deg/sec expressed in an inertial reference frame. Under the effect of the gravity gradient, which is a conservative force, the object will rotate endlessly along the three axis. The object is then subjected to a magnetic field $\vec{B} = [0, 150, 0]$ μT expressed in an orbital reference frame. This reference frame has its origin in the COG of the object, the X axis points in the nadir direction, the Y axis points in the along track velocity and the Z axis is perpendicular to the orbital plane.

The results obtained show that the three components are reduced below 2 deg/sec after 20 days. Figure 18 shows the evolution of the angular velocity vector, between the target body reference frame and the orbital reference frame, expressed in the orbital frame. This is the velocity seen by the chaser spacecraft which has to be damped before the capturing process. The magnetic field vector points towards the along track direction, that is why, the Z component of the angular velocity (perpendicular to the orbital frame) is damped more quickly than the other two.

Figure 19 shows the torques induced on the target object. Assuming that the magnetic field induced on the target is constant and homogenous, the same torques with

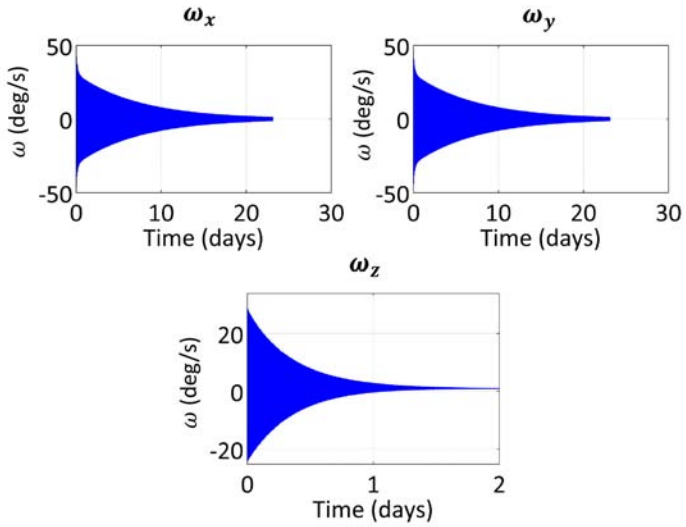

Figure 18: Rotational velocity of the target object of its body frame w.r.t to the orbital reference frame expressed in the orbital frame.

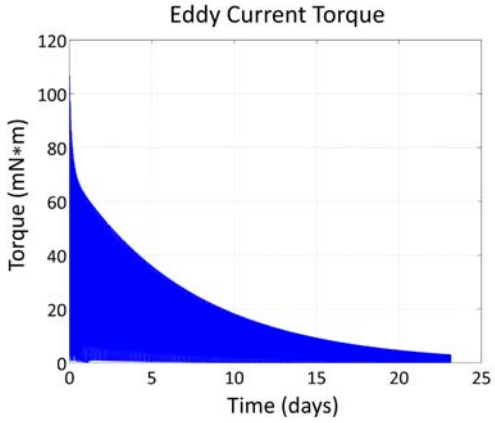

Figure 19: Torques induced by the eddy currents on the target object.

opposite direction will appear on the chaser and they have to be counteracted.

4.6. Spatial Gradient of the magnetic field

In the previous mathematical development a homogeneous magnetic field was considered. However, for the first design presented for the de-tumbling process (see Figure 9), the chaser spacecraft has just one electromagnetic coil which has dimensions of the same order of magnitude of the size of the space debris object. Therefore, for this design, the spatial gradient of magnetic field can not be neglected.

This will have two main consequences on the interaction between the chaser and the target object. First of all, a reduction in the efficiency of the de-tumbling process will take place and this is quantified, in an approximate way, by introducing an efficiency factor on the Magnetic Tensor (see Section 4.6.1). Secondly, net forces between the chaser and the target will appear (see Section 4.6.2).

The diverse effects of the spatial non-uniformity of the magnetic field are only outlined here and a deeper analysis will continue in future work. This will require an extensive analysis due to the large number of parameters that must be considered: the radius and distance of the magnetic coil, the geometry of the target, the variable attitude of target with respect to the chaser in time, etc.

4.6.1. Effective Magnetic Tensor

In order to analyse the non-uniformity of the magnetic field, an effective magnetic tensor M_{eff} is defined under several simplifying hypotheses explained below. M_{eff} is related to the magnetic tensor M expressed in its principal axes through some coefficients μ_{effi}:

$$M_{eff} = \begin{bmatrix} \mu_{eff1}M_1 & 0 & 0 \\ 0 & \mu_{eff2}M_2 & 0 \\ 0 & 0 & \mu_{eff3}M_3 \end{bmatrix}. \quad (80)$$

The following simplifications are taken into account:

1. The gradient of the magnetic field is assumed to be small enough to linearise the magnetic field $\vec{B}$ around the COG of the body,

$$\vec{B} = \vec{B}_G + \left.\frac{\partial \vec{B}}{\partial \vec{r}}\right|_G (\vec{r} - \vec{r}_G). \quad (81)$$

Using Equation (81), up to a first order approximation, the magnetic moment is expressed as:

$$\vec{m} = M_{eff}(\vec{\omega} \times \vec{B}_G) = M_{eff}\vec{\Omega}_G, \quad (82)$$

where B_G is the magnetic field at the COG of the body.

2. It will be assumed that $\vec{\Omega} = \vec{\omega} \times \vec{B} = \Omega\vec{n}$ is oriented along one of the principal directions of the magnetic tensor so that,

$$\vec{m} = M_{effi}\vec{\Omega}_G = \mu_{effi}M_i\vec{\Omega}_G, \quad (83)$$

being M_{effi} one of the eigenvalues of the effective magnetic tensor.

3. It is assumed that the geometry of the target body is such that the distribution of eddy current loops lie on flat planes ($\vec{n}$ =constant).

The second and third hypotheses are true for a spherical shell for any orientation of $\vec{\Omega}$. Therefore, the proposed analysis may be adequate for quasi-spherical shells. More specifically, it will be considered in the following mathematical development that the target body is an ellipsoidal shell with its three semi-axes similar in size, subject to a magnetic field $\vec{B}(\vec{r})$ symmetric with respect to one of the planes of symmetry of the ellipsoid (see Figure 20).

The magnetic flux φ given by Faraday's law is (Vanderlinde, 2004):

$$\varphi = \iint_{S_0} \vec{n} \cdot \vec{B} dS_0 = \vec{n} \cdot \iint_{S_0} \vec{B} dS_0 = S_0 \vec{n} \cdot \vec{B}_{eff}, \quad (84)$$

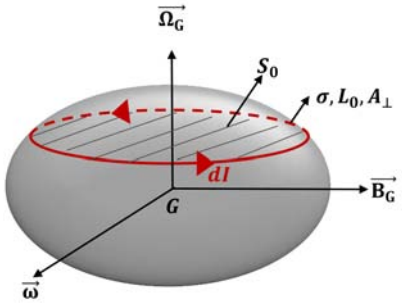

Figure 20: Ellipsoid quasi-spherical shell.

where $\vec{B}_{eff} = \frac{1}{S_0}\iint_{S_0} \vec{B} dS_0$.

Assuming a non-uniform magnetic field but constant in time, $\dot{\varphi}$ is obtained as:

$$\dot{\varphi} = \iint_{S_0} (\vec{\omega} \times \vec{n}) \cdot \vec{B} dS_0 =$$
$$= -(\vec{n} \times \vec{\omega}) \cdot \iint_{S_0} \vec{B} dS_0 = -S_0\vec{n}(\vec{\omega} \times \vec{B}_{eff}) = -S_0\Omega_{n,eff}. \quad (85)$$

The vector $\vec{n}$ has the direction $\vec{n}_G = \frac{\vec{\Omega}_G}{\Omega_G}$ where $\vec{\Omega}_G = \vec{\omega} \times \vec{B}_G$ and G is the COG of the body. Two new variables are defined $\Omega_{n,eff}$ and ρ_{eff} as:

$$\Omega_{n,eff} = \vec{n}_G \cdot (\vec{\omega} \times \vec{B}_{eff}), \quad (86)$$

$$\rho_{eff} = \frac{\Omega_{n,eff}}{\Omega_G}. \quad (87)$$

Lenz's Law establishes the relationship between the electromotive force (e.m.f) and the magnetic flux (88). Considering this relationship and using Equation (85), the e.m.f. can be written as:

$$\varepsilon = -\frac{d\varphi}{dt} = S_0\Omega_{n,eff}, \quad (88)$$

In addition, Ohm's Law gives the relationship between the e.m.f. and the current intensity I for one conductive circuit, as voltage divided by the resistance of the circuit:

$$I = \frac{\varepsilon}{L_0/\sigma A_\perp} = \varepsilon\sigma\frac{V_0}{L_0^2} = \sigma\frac{S_0V_0}{L_0^2}\Omega_{n,eff}, \quad (89)$$

where $A_\perp$ is the cross section of the electrical circuit, L_0 is its longitude and $V_0 = A_\perp L_0$ is its volume.

Now, considering $A_\perp$ and therefore, V_0 as infinitesimal magnitudes, the intensity of each eddy current loop, can be expressed as:

$$dI = \sigma\frac{S_0}{L_0^2}\Omega_{n,eff}dV_0 \quad (90)$$

and the induced magnetic moment in each eddy current loop is:

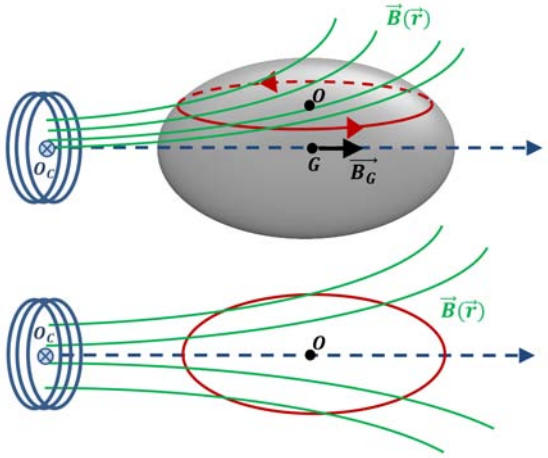

Figure 21: Non homogeneous magnetic field on a quasi-spherical body.

$$d\vec{m} = S_0\vec{n}_G dI = \sigma\frac{S_0^2}{L_0^2}dV_0\rho_{eff}\vec{\Omega}_G = \frac{\sigma}{4}R_0^2\rho_{eff}dV_0\vec{\Omega}_G, \tag{91}$$

where $R_0 = \frac{2S_0}{L_0}$ is the mean radius of the differential eddy current loop. Integrating the magnetic moment over the whole volume and taking into account Equation (82), each eigenvalue of the effective magnetic tensor acquires the form:

$$M_{effi} = \frac{\sigma}{4}\int_{V0}\rho_{eff}R_0^2dV_0 = \mu_{effi}M_i, \tag{92}$$

Since M_i must be obtained when $\rho_{eff} = 1$, the correction factor μ_{eff} for each eigenvalue of the magnetic tensor M can be written as:

$$\mu_{eff} = \frac{M_{effi}}{M_i} = \frac{\int_{V_0}\rho_{eff}R_0^2dV_0}{\int_{V_0}R_0^2dV_0}, \tag{93}$$

The factor ρ_{eff} defined in (87) is developed further in (94). It must be noted that when computing $\vec{B}_{eff}\times\vec{n}_G$ in each S_0, only the components of $\vec{B}_{eff}$ parallel to S_0 are necessary, since the normal to the surface S_0 is precisely $\vec{n}_G$. In addition, the average of $\vec{B}_{eff}\times\vec{n}_G$ perpendicular to $\vec{B}_G$ can be considered null due to the hypotheses considered. This condition occurs because the magnetic field and the object are symmetric with respect to the plane $O_c - G - O$, where O_c is the center of the magnetic coil and O is the COG of the surface S_0 (see Figure 21).

$$\rho_{eff} = \frac{\Omega_{n,eff}}{\Omega_G} = \frac{\vec{n}_G\cdot(\vec{\omega}\times\vec{B}_{eff})}{\vec{n}_G\cdot(\vec{\omega}\times\vec{B}_G)} = \frac{\vec{n}_G\times\vec{B}_{eff}}{\vec{n}_G\times\vec{B}_G} = \\ = \frac{\iint_{S_0}\vec{B}\cdot\vec{B}_G dS_0}{B_G^2 S_0}. \tag{94}$$

Further simplification may be obtained if the gradient of the $\vec{B}(\vec{r})$ is small enough to linearise the field around point O. Then $\vec{B} = \vec{B}_0 + \left.\frac{\partial\vec{B}}{\partial\vec{r}}\right|_0(\vec{r}-\vec{r}_0)$ and the parameters ρ_{eff} and μ_{eff} become:

$$\rho_{eff} \approx \frac{\vec{B}_0\cdot\vec{B}_G}{B_G^2}, \tag{95}$$

$$\mu_{eff} \approx \frac{\int_{V_0}\frac{\vec{B}_0\cdot\vec{B}_G}{B_G^2}R_0^2dV_0}{\int_{V_0}R_0^2dV_0}. \tag{96}$$

In the case of a spherical shell, this efficiency factor μ_{eff} becomes:

$$\mu_{eff} = \frac{3}{2}\int_0^{\pi/2}\frac{\vec{B}_0\cdot\vec{B}_G}{B_G^2}\sin^3\alpha d\alpha. \tag{97}$$

where α is the azimuthal spherical coordinate. Figures 22 and 23 show how the efficiency factor varies for different coil sizes and relative distances between the magnetic coil and the target surface. The two cases analysed correspond to a spherical shell of 2 meters and 5 meters respectively. The reason why the efficiency factor increases with the relative distance is that the magnetic field becomes more homogeneous inside the target domain. The torque induced on the space debris object is linear with respect to the effective Magnetic Tensor, which increases with the distance, and it is also proportional to the square of the magnetic field, which diminishes with the distance. The decrease of the magnetic field outcomes the effect of the efficiency factor as shown in Figure 24 and therefore, it is still more convenient to place the coil as close as possible to the target object to enhance the de-tumbling process.

For a relative distance between the magnetic coil and the target surface of 5 meters, the efficiency is above 95% in the first case and 85% in the second case. This first analysis shows that the loss of efficiency due to the spatial gradient of the magnetic field may not be drastic and that the first design presented for the de-tumbling process (Figure 9) could be a viable option. Nonetheless, due to the simplifying hypotheses carried out, the results here provided, should not be regarded as definitive. It does, however, show that the first design can not be discarded a priori. Consequently, this first analysis may serve as the basis for further investigation on the geometries of real space debris objects.

4.6.2. Magnetic force

Another consequence of the non-uniformity of the magnetic field is the appearance of net forces between the chaser and the target object. This effect is analysed using perturbations theory by expanding in Taylor series the magnetic field about the center of gravity of the target object (Boyer, 1988; Vanderlinde, 2004),

$$\vec{B} = \vec{B}_G + \Lambda_G(\vec{r}-\vec{r}_G). \tag{98}$$

$\vec{B}_G$ is the value of the magnetic field at the center of gravity G of the target, $\vec{r}_G$ is the position vector of the

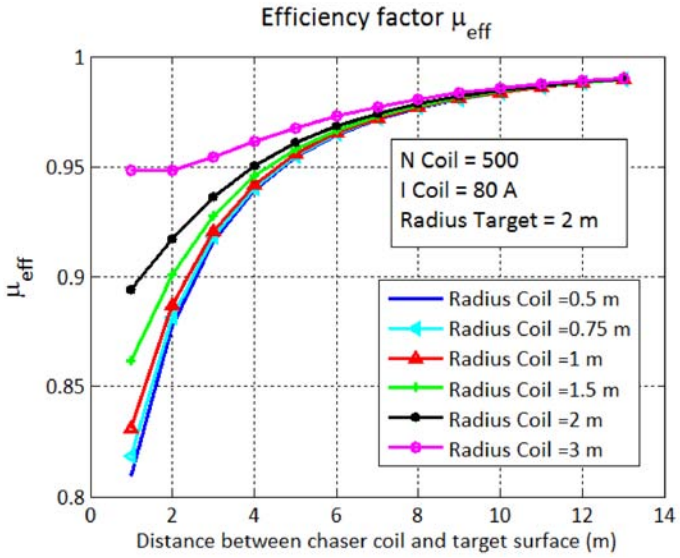

Figure 22: μ_{eff} for a spherical shell of 2 metres of radius subject to a magnetic field induced by an electromagnetic coil with an intensity of 80 A and 500 turns of wire for different radius of the coil and different relative distances between the coil and the target surface.

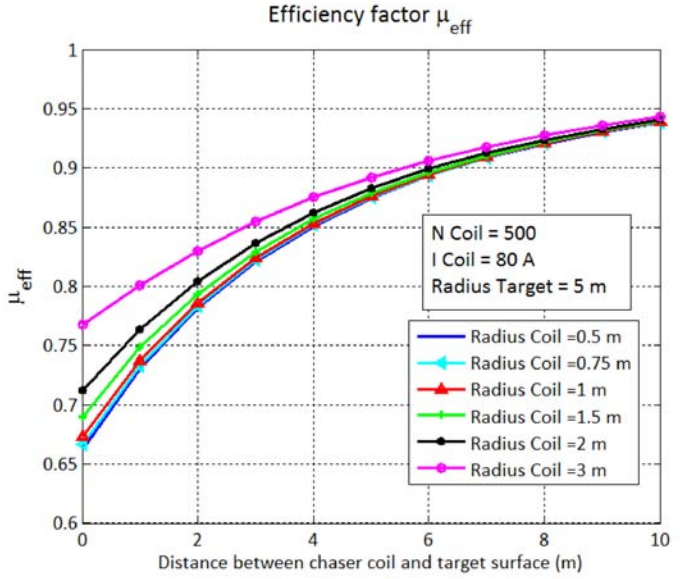

Figure 23: μ_{eff} for a spherical shell of 5 metres of radius subject to a magnetic field induced by an electromagnetic coil with an intensity of 80 A and 500 turns of wire for different radius of the coil and different relative distances between the coil and the target surface.

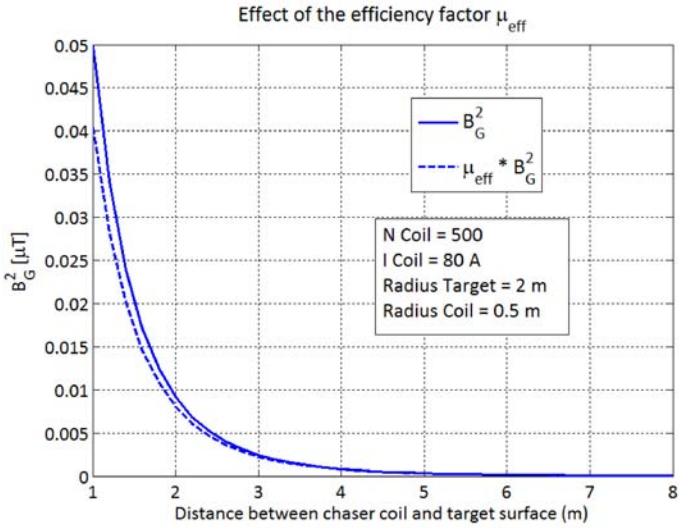

Figure 24: Magnetic field at the COG of the target for different relative distances with and without efficiency factor.

COG and Λ_G is the Jacobian matrix which contains the partial spatial derivatives of the magnetic field particularised at the COG of the target $\Lambda_{ij} = \frac{\partial B_i}{\partial r_j}\Big|_G$. Introducing this term in the general Lorentz force formula, the following expression for the force is reached (Boyer, 1988):

$$\vec{F} = \int \vec{j} \times \vec{B} dV = \overbrace{\int \vec{j} \times \vec{B}_G dV}^{I_1=0} + \int \vec{j} \times \Lambda_G(\vec{r} - \vec{r}_G) dV \Rightarrow$$
$$\Rightarrow \vec{F} = \Lambda_G^T \vec{m}. \tag{99}$$

The first integral I_1 is zero as there are no induced forces if the magnetic field is homogeneous (Boyer, 1988) ($\vec{B}_G = const.$). In addition, the Jacobian matrix is a symmetric matrix. This is proved as follows. The electrical currents on the electromagnetic coil of the chaser $\vec{j}_c$, generate a magnetic field $\vec{H} = \frac{1}{\mu}\vec{B}$ that follows Maxwell equations:

$$\nabla \times \vec{H} = \vec{j}_c + \frac{\partial}{\partial t}(\epsilon \vec{E}), \tag{100}$$

$$\nabla(\mu \vec{H}) = 0, \tag{101}$$

where ϵ is the electric permittivity and μ the magnetic permeability. In free space, outside the source, Equation (100), turns out to be $\nabla \times \vec{H} = \vec{0}$ and therefore, $\vec{H} = -\nabla\zeta$, where ζ is the magnetic scalar potential (Vanderlinde, 2004). Assuming a constant value for the magnetic permeability μ,

$$\vec{B} = -\mu \frac{\partial \zeta}{\partial \vec{r}} \tag{102}$$

and Jacobian matrix acquires the form,

$$\Lambda_{ki} = \frac{\partial B_k}{\partial r_i} = -\mu \frac{\partial^2 \zeta}{\partial r_i \partial r_k} = \Lambda_{ik}, \tag{103}$$

Therefore, $\Lambda = \Lambda^T$ is a symmetric matrix and the force is:

$$\vec{F} = \Lambda_G \vec{m}. \tag{104}$$

Considering the relationship between the magnetic moment $\vec{m}$ and the effective magnetic tensor M_{eff}, given by (82), the final formula of the force is expressed as:

$$\vec{F} = \Lambda_G (M_{eff}(\vec{\omega} \times \vec{B}_G)) = \Lambda_G M_{eff} \vec{\Omega}. \tag{105}$$

This implies that the force given by (105) can be expressed by means of one single matrix $(\Lambda_G M_{eff})$.

5. Conclusions and Future Work

A general method is presented in this paper to evaluate the torque induced by the eddy currents due to a uniform and constant magnetic field. The method is based on the computation of a new tensor called the 'Magnetic Tensor' which depends on how the conductive mass is distributed throughout the body. The general theory to compute this tensor by Finite Element Method is given as well as a specific model based on bars called Frame Model. This last method provides us with an explicit formula to evaluate the magnetic tensor. Analytical solutions for the spherical shell, the open cylindrical shell and flat plates are given for the magnetic tensor and the models are validated with existent published work.

The analysis presented on the eddy current torque generalizes the existent analytical solutions which are only valid for specific orientations of the angular velocity vector and the magnetic field. In addition, the use of the magnetic tensor simplifies the computation of the eddy current torque because it avoids solving the Poisson equation with Neumann conditions in each time step of the integration of Euler equations, for any type of body.

The second part of the paper presents an active de-tumbling method based on eddy currents for space debris objects. The existent active debris removal methods that require physical contact with the target are not able to capture objects which are rotating faster than a few degrees per second. Therefore, a de-tumbling phase prior to the capturing phase may be needed.

The main advantage of the method presented is that it requires no mechanical contact with the target. Different designs for the de-tumbling system are discussed with the conclusion that the simplest design consists on a single fixed-size coil on the chaser placed at a certain distance from the target. This will inevitably generate a non-homogeneous magnetic field. This effect will result in a loss of efficiency which depends on the dimensions of the target object, the magnetic coil on the chaser and the relative distance between both objects. The analysis carried out for a quasi-spherical object shows that the efficiency penalty may be around 5% to 10% for a relative distance of 5 meters between the coil and the target surface. The second consequence of the having a non-homogeneous magnetic field, is the appearance of net forces between the chaser spacecraft and the target object. An explicit formula is reached for this force based on an effective magnetic tensor.

The article also includes an analysis of the characteristic time of decay and the possible induced precession on the target object. The characteristic time of decay of the rotational speed of the target varies with the inverse square of the magnetic field and also depends on the ratio of conductive versus non-conductive material of the object.

Furthermore, the article contains a case study based on an Ariane H10 upper stage. Upper stages could be adequate targets for the de-tumbling based on the eddy currents due to their high ratio of conductive material. A simulation has been run for an object in a LEO orbit under the effect of the gravity gradient and the induced eddy current torque by the chaser, under the assumption of a homogenous and constant magnetic field. The results show how the three components of the angular velocity vector are damped within 20 days.

All in all, approximate mathematical models for the mechanical interactions (forces and torques) of the chaser-target system due to the eddy currents phenomenon have been established in this work. Further investigation needs to be carried out on the effect of the spatial gradient of the magnetic field, taking into account geometries of existing space debris objects. Future simulations with additional perturbations other than the gravity gradient will be performed, including the effect of having ferromagnetic material on the target object. At present, a full systems-engineering analysis of the de-tumbling process based on eddy current is being developed and experimental tests are currently being carried out to further validate the mathematical models.

6. Acknowledgements

The research work that is being developed at Southampton University in the United Kingdom as part of the European Union Framework 7 Program, Marie Curie Initial Training Networks (ITN) project 'Stardust' (Stardust, 2013) . This network is led by Professor Massimiliano Vasile at the University of Strathclyde in Glasgow, Scotland.

7. Vitae

Natalia Ortiz Gómez received an M.Sc. in Aeronautical Engineering from Polytechnic University of Madrid (ETSIA-UPM) in 2009. She worked at GMV, Spain, in the Mission Analysis department for two years until 2011.

Afterwards, she worked for two additional years at the European Space Agency, The Netherlands, at the Concurrent Design Facility (CDF) under the Spanish Trainee Programme. In 2013, she started her Ph.D. at Southampton University, UK, as part of the European Union Framework 7 Program, project 'Stardust'. Her area of research focuses on the analysis of the tumbling of space debris objects and a de-tumbling method based on eddy currents.

Scott James Ian Walker is a Lecturer in Astronautics. He received his PhD from the University of Southampton, Southampton, UK, in 2004. His expertise is in Spacecraft Attitude Control, Aerospace Structures, Deployable Structures, Morphing Structures, Structural Dynamics and has published 13 Journal Papers, 22 Conference Papers and was awarded the Jefferson Prize in 2003. He is currently active in two FP7 projects the EU FP7 Marie Curie ITN 'Stardust' Project and EU FP7 ROV-E Project. He has undertaken consultancy for Airbus DS, and Surrey Satellite Technology Limited (SSTL).

A. Proof of the symmetry of the Magnetic Tensor

In Section 3.2, a general proof of the symmetry of the Magnetic Tensor based on Onsager's Theorem has been included. In this section, a general confirmation of the symmetry of the Magnetic Tensor has been developed.

The general solution to Equations (2,3,4) is split as a sum of a homogeneous and a particular solution for $\vec{j}$:

$$\vec{j} = \vec{j}^{(part)} + \vec{j}^{(hom)} = \frac{\sigma}{2}\vec{\Omega} \times \vec{r} - \sigma\nabla\psi, \tag{106}$$

Therefore, the magnetic moment induced on the target object can also be split in the same way:

$$\begin{aligned} \vec{m} = \frac{1}{2}\int_V \vec{r} \times \vec{j} dV = \\ = \vec{m}^{(part)} + \vec{m}^{(hom)} = (M^{(part)} + M^{(hom)})\vec{\Omega}. \end{aligned} \tag{107}$$

In addition, the general equations for ψ are expressed as a function as a new parameter $\vec{t} = \vec{n}_v \times \vec{r}$:

$$\Delta\psi = 0 \;\; in \; V, \tag{108}$$

$$\frac{\delta\psi}{\delta n_v} = -\frac{1}{2}(\vec{r} \times \vec{\Omega}) \cdot \vec{n}_v = -\frac{1}{2}\vec{\Omega} \cdot \vec{t} \;\; in \; \partial V. \tag{109}$$

First of all, the general solution of $\vec{M}^{(part)}$ is obtained as follows:

$$\begin{aligned} \vec{m}^{(part)} = \frac{\sigma}{4}\int_V \vec{r} \times (\vec{\Omega} \times \vec{r}) dV = \\ = \frac{\sigma}{4}\left[r^2 I - \vec{r}\vec{r}^T dV\right]\vec{\Omega}, \end{aligned} \tag{110}$$

$$M^{(part)} = \frac{\sigma}{4}\int_V (r^2 I - \vec{r}\vec{r}^T) dV, \tag{111}$$

where I is the identity matrix. It can be easily seen that $M^{(part)}$ in (111) is symmetric, that is, $M^{(part)} = (M^{(part)})^T$.

Second of all, the general solution for the homogeneous part of the Magnetic Tensor $\vec{M}^{(hom)}$ can be obtained as follows. The homogeneous part of the magnetic moment is:

$$\vec{m}^{(hom)} = -\frac{\sigma}{2}\int_V \vec{r} \times \nabla\psi dV. \tag{112}$$

In addition, the general solution for Equations (108,109) can be expressed as:

$$\forall \vec{r} \; in \; V: \;\; \psi(\vec{r}) = \psi_0 + \int_{\vec{s} \in \partial V} G_N(\vec{r}, \vec{s}) \frac{\partial\psi(\vec{s})}{\partial n_v} dS. \tag{113}$$

$$\forall \vec{s} \; in \; \partial V: \;\; \psi(\vec{s}) = \psi_0 + \int_{\vec{s}' \in \partial V} G_N(\vec{s}, \vec{s}') \frac{\partial\psi(\vec{s}')}{\partial n_v} dS', \tag{114}$$

where ψ_0 is an arbitrary constant and $G_N(\vec{s}, \vec{s}')$ is a Green function of the Neumann problem. The constant $\psi_0 = \int_{\vec{s}' \in \partial V} F(\vec{s}') \frac{\partial\psi(\vec{s}')}{\partial n_v} dS'$ can be chosen in such a way that $G(\vec{s}, \vec{s}') = G_N(\vec{s}, \vec{s}') + F(\vec{s}')$ is symmetric, that is, $G(\vec{s}, \vec{s}') = G(\vec{s}', \vec{s})$ (Jackson, 1999).

Below, the convention of summation over repeated indices is used. It holds that:

$$\frac{\partial(e_{ijk}x_j\psi)}{\delta x_k} = \underbrace{e_{ijk}\partial_{ij}\psi}_{0} + e_{ijk}x_j\frac{\partial\psi}{\partial x_k}. \tag{115}$$

Therefore, $\vec{m}^{(hom)}$ can be written as:

$$m_i^{(hom)} = -\frac{\sigma}{2}\int_V \frac{\partial(e_{ijk}x_j\psi)}{\partial x_k} dV. \tag{116}$$

Now, applying the Divergence Theorem (Vanderlinde, 2004) to Equation (116) and making use of the boundary condition (109):

$$\begin{aligned} m_i^{(hom)} = -\frac{\sigma}{2}\int_{\partial V} e_{ijk}x_j n_k \psi dS \Rightarrow \\ \Rightarrow \vec{m}^{(hom)} = \frac{\sigma}{2}\int_{\vec{s} \in \partial V} \vec{t}(\vec{s}) \cdot \psi(\vec{s}) dS. \end{aligned} \tag{117}$$

Then, introducing Equation (114) in (117):

$$\begin{aligned} m_i^{(hom)} = \frac{\sigma}{2}\int_{\vec{s}' \in \partial V} t_i(\vec{s}) \cdot \int_{\vec{s}' \in \partial V} G(\vec{s}, \vec{s}') \frac{\partial\psi(\vec{s}')}{\partial n_v} dS' dS = \\ = -\frac{\sigma}{4}\int_{\vec{s} \in \partial V}\int_{\vec{s}' \in \partial V} t_i(\vec{s}) G(\vec{s}, \vec{s}') t_j(\vec{s}') \Omega_j dS' dS. \end{aligned} \tag{118}$$

Finally, the homogeneous part of the Magnetic Tensor is obtained in Equation (119) which also shows its symmetrical character:

$$M_{ij}^{(hom)} = -\frac{\sigma}{4}\int_{\vec{s}\in\partial V}\int_{\vec{s}'\in\partial V} t_i(\vec{s})G(\vec{s},\vec{s}')t_j(\vec{s}')dS'dS = M_{ji}^{hom} \tag{119}$$

All in all, the Magnetic Tensor is symmetric and it has the form:

$$M = \frac{\sigma}{4}\int_V (r^2 I - \vec{r}\vec{r}^T)dV - \\ -\frac{\sigma}{4}\int_{\vec{s}\in\partial V}\int_{\vec{s}'\in\partial V} G(\vec{s},\vec{s}')\vec{t}(\vec{s})\vec{t}^T(\vec{s}')dS'dS = M^T. \tag{120}$$

Johnson Space Center, National Aeronautics and Space Administration, NASA Orbital Debris Program Office (2014), URL:http://orbitaldebris.jsc.nasa.gov/, Accessed: 11–08–2014.

Francois La Porte & Eloy Sasot, Operational management of collision risks for LEO satellites at CNES, Space–Ops 2008 Conference, AIAA-2008–3409.

Carmen Pardini & Luciano Anselmo, Review of past on-orbit collisions among cataloged objects and examination of the catastrophic fragmentation concept, DOI: 10.1016/j.actaastro.2014.03.013, Acta Astronautica, Volume 100, pages 30–39, 2014.

Christophe Bonnal, Jean-Marc Ruault & Marie-Christine Desjean, Active debris removal: Recent progress and current trends, DOI: 10.1016/j.actaastro.2012.11.009, Acta Astronautica, Volume 85, pages 51–60, 2013.

Luisa Innocenti, Tiago Soares & Jessica Delaval, ESA Clean Space Initiative, 6th European Conference on Space Debris (Darmstadt), April 2013.

Marco Castronuovo, Active space debris removalA preliminary mission analysis and design, DOI: 10.1016/j.actaastro.2011.04.017, Acta Astronautica, Volume 69, pages 848–859, issue 9–10, 2011.

Lee Jaspera & Hanspeter Schaubb, Input Shaped Large Thrust Maneuver with a Tethered Debris Object, DOI: 10.1016/j.actaastro.2013.11.005, Acta Astronautica, Volume 96, pages 128–137, 2014.

Kjetil Wormnes, J.H. de Jong, Holger Krag & Gianfranco Visentin, Throw- nets and Tethers for Robust Space Debris Capture, DOI: 10.1016/j.actaastro.2013.11.005, IAC–13, A6.5, 2x16445, 64th International Astronautical Congress, Beijing, China 2013.

Prasad K. Kadaba, Feasibility of Noncontacting Electromagnetic Despinning of a Satellite by Inducing Eddy Currents in Its Skin-Part I: Analytical Considerations, IEEE Transactions on Magnetics Vol 31, Num. 4. July 1995.

Fuhimito Sugai, Development of an Eddy Current Brake System for Detumbling Malfunctioning Satellites IEEE/SICE International Symposium on System Integration (SII) Kyushu University, Fukuoka, Japan, December 2012.

Louis Smith, A Theoretical Study of the Torques induced by a Magnetic Field on Rotating Cylinders and Spinning Thin–wall Cones, Cone Frustums, and General Body of Revolution, Rep. Number R–129, Planetary and Space Science, National Aeronautics and Space Administration, 1962.

J. F. A. Ormsby, Eddy Current Torques and Motion Decay on Rotating Shells, Project 8051, United States Air Force, 1967.

Peter C. Hughes, Spacecraft Attitude Dynamics, Dover Publications, 2004.

L.D. Landau & E.M. Lifshitz, Electrodynamics of continuous media, Course of Theoretical Physics Volume 8, Pergamon Press, 1984.

J. Vanderlinde, Classical Electromagnetic Theory, Second Edition, Kluwer Academic Publishers, 2004.

V. Williams & A. J. Meadows, Eddy current torques, air torques, and the spin decay of cylindrical rocket bodies in orbit, DOI: 10.1016/0032-0633(78)90003-X, Planetary and Space Science, Volume 26, pages 721–726, issue 8, 1978.

E. Y. Yu, Spin Decay, Spin-Precession Damping, and Spin-Axis Drift of the Telstar Satellite, Volume 42, pages 2169–2193, issue 5, The Bell System Technical Journal, 1963.

H. Boehnhardt, H. Koehnhke & A. Seidel, The acceleration and the deceleration of the tumbling period of Rocket Intercosmos 11 during the first two years after launch, Volume 162, pages 297–313, issue 2, Astrophysics and Space Science, 1989.

Nicolas Praly, Mathieu Hillion, Christophe Bonnal, Julien Laurent-Varin & Nicolas Petit, Study on the eddy current damping of the spin dynamics of space debris from the Ariane launcher upper stages, DOI: 10.1016/j.actaastro.2012.03.004, Acta Astronautica, Volume 76, pages 145–153, 2012.

Frederick Reif, Fundamentals of Statistical and Thermal Physics, McGraw-Hill, 1965.

O. C. Zienkiewicz, The Finite Element Method, 3rd Edition, McGraw-Hill, 1978.

S. Timoshenko & J. N. Goodier, Theory of Elasticity, McGraw-Hill, 1934.

H.F. Weinberger, A first course in Partial Differential Equations with Complex Variables and Transform Methods, Dover Publications, 1995.

Weijia Yuan, Second-Generation High-Temperature Superconducting Coils and Their Applications for Energy Storage, Springer, 2011.

Gwendolyn V. Gettliffe, Niraj K. Inamdar, Rebecca Masterson & David W. Miller, High-Temperature Superconductors as Electromagnetic Deployment and Support Structures in Spacecraft, NASA NIAC Phase I, Final Report, MIT Space Systems Lab, January 2012.

Ronny Votel & Doug Sinclair, Comparison of Control Moment Gyros and Reaction Wheels for Small Earth-Observing Satellites, 26th Annual AIAA/USU Conference on Small Satellites, Logan, Utah, 2012.

R. Battison, W.j: Burguer, V. Calvalli, R. Musenich et al. Active Magnetic Shielding for Long Duration Manned Space Missions, Proceedings 6th IAASS International Space Safety Conference, Montreal, May 2013.

National Aeronautics and Space Administration, Assessment and control of Spacecraft Magnetic Fields, NASA SP-8037, September 1970.

N2YO Webpage, Real Time Satellite Tracking and Prediction, 2006, URL:http://www.n2yo.com/.

European Space Agency, Space Engineering Structural materials handbook part 3: Load transfer and design of joints and design of structures, European Cooperation on Space Standardization, ECSS–E–HB–32–20 Part 3A, March 2011.

Arianespace S.A., Ariane 4 user's manual, Issue 2, February 1999.

Arianespace S.A., Ariane 5 user's manual, Issue 5, Revision1, July 2011.

P. Papushev, Yu. Karavaev & M. Mishina, Investigations of the evolution of optical characteristics and dynamics of proper rotation of uncontrolled geostationary articial satellites, Advances in Space Research, Volume 43, pages 1416–1422, issue 9, 2009.

H. T. Boyer, The Force on a Magnetic Dipole, American Journal of Physics, Volume 56, Pages 688–692, Issue 8, 1988.

Stardust Programme: Advanced Research Network on Asteroid and Space Debris Manipulation, European Union Framework 7 Program, Marie Curie Initial Training Networks (ITN), 2013, URL: http://www.stardust2013.eu/.

John David Jackson, Classical Electrodynamics, John Wiley & Sons, New York, 3rd Edition, 1999.